Nature of the structural and dynamical disorder in organic cocrystals with a true nanometric size channel-like architecture

Luisa Roca-Paixão[1], Natália T. Correia[1], Florence Danède[1], Maria T. Viciosa[2], Alexander Lee Morritt[3], Yaroslav Z. Khimyak[3], Frédéric Affouard[1*]

[1] Univ. Lille, CNRS, INRAE, Centrale Lille, UMR 8207 - UMET - Unité Matériaux et Transformations, F-59000 Lille, France

[2] Centro de Química Estrutural, Institute of Molecular Sciences, Department of Chemical Engineering, Instituto Superior Técnico, Universidade de Lisboa, Av. Rovisco Pais 1049-001 Lisbon, Portugal.

[3]School of Pharmacy, University of East Anglia, Norwich Research Park, Norwich, NR4 7TJ, United Kingdom.

*Corresponding author: frederic.affouard@univ-lille.fr

Abstract

The nature of the structural and dynamical disorder of the nanoporous organic cocrystal carbamazepine-tartaric acid designed by liquid assisted grinding is investigated through complementary solid-state NMR, X-ray diffraction and broadband dielectric spectroscopy experiments combined with molecular dynamics simulations. In this article, we especially highlight that the tartaric acid molecules present in the channel-like cocrystalline architecture show both translational and rotational dynamical disorder. Such a disorder seems only partial since tartaric acid molecules are strongly hydrogen-bonded to the carbamazepine molecules which form the channels and they thus share with them some order. Tartaric acid species are organized as one-dimension interrupted single files of molecules weakly hydrogen bonded between them. Translational dynamics occurs by small hops of about 6 to 7 Å consistent with the distance between first neighbors. At short times, it can be described as a single-file diffusion process while at longer times the classical diffusion (Fickian) is recovered. Random motions are explained by the presence of several short single files of molecules in the channel instead of just one single file. Rotational dynamics is interpreted as rotational jumps between preferred orientations. It gives rise to a change of the molecular dipole moments orientations, which are detected by dielectric relaxation spectroscopy. Freezing out of the rotational molecular mobility is detected in the temperature range [173-193] K concomitantly with the presence of a kink in the temperature evolution of the crystalline cell volume which is usually associated with the glass transition phenomenon. It reveals a remarkable link between the molecular mobility of the tartaric acid molecules and the overall crystal anharmonicity. The present findings aim to demonstrate the interest of disordered channel-like cocrystals for investigation of dynamics in nanoconfinement environments.

Key words: nanoporous materials, carbamazepine, cocrystal, disorder, molecular dynamics simulation, dielectric relaxation spectroscopy

INTRODUCTION

Investigation of the molecular mobility of small organic molecules (water, urea, alkanes alcohols, polyols, sugars, pharmaceuticals…) or even large biomolecules (peptides, proteins) in various confinement environments has attracted a lot of considerations for several years, from the fundamental physics point of view as well as for its relevance to biology, geology, and materials science for technological applications.[1–4] Indeed, dynamical properties of fluids, as well as their structural and thermodynamical properties, can be significantly altered by their confining environments compared to those of bulk fluids. The degree of alteration is strongly dependent on the geometry imposed by the shape and the size of the pores and the nature of the interactions between the molecules and the surface of the host medium. Very diverse inorganic and organic confining environments are reported in the literature. For example, many works have been performed using mesoporous silica matrices,[5–10] single-crystal beryl mineral silicates,[11,12] metal−organic frameworks,[13,14] zeolites,[15–21] carbon nanotubes,[22–24] nanoporous organic intergrowth crystals,[25] cyclodextrin nanocavities,[26–28] crystalline columnar assembly of macrocycles,[29] transmembrane cyclic peptide nanotubes,[30,31] block copolymer nanochannels,[32,33] ion channels in cell membranes,[34] phospholipid membranes,[35] graphene slit pores,[36] to cite only a few. Most studies of confined fluids have mainly focused on porous media larger than 1 nm. For extreme confining environments made of unidimensional channels of very narrow size of about 1 nm or less, the restricted geometry makes mutual passage between the molecules forbidden, and as a result, the sequence of molecules remains the same over time. This feature makes molecular diffusion nonconventional compared to that of isotropic diffusion in the bulk system and it is known as single-file diffusion. The microscopic

origin of this unusual diffusion still remains unclear. In some cases, an intriguing transition from this single-file diffusion to the classical diffusion mechanism (Fickian) has been also reported at longer times depending on the length of the pores.[10,12–16,18,19,24,27,29]

In this work, we aim to show that cocrystals may also offer a new type of interesting confinement environments including the possibility to investigate rotational and translational dynamics in a true nanometric size channel-like architecture. Cocrystals[37–45] are molecular solids that are neutral crystalline single-phase materials composed of two or more different molecular compounds associated via weak supramolecular interactions such as van der Waals, hydrogen, halogen or π-π stacking. Cocrystals have shown a considerable increase of interest in recent years due to their possibility to improve many properties of pharmaceuticals such as aqueous solubility, dissolution rate, hygroscopicity bioavailability, or mechanical properties. This interest is particularly demonstrated by the number of structures submitted to the Cambridge Structural Database.[46] While most of the cocrystals are fully ordered materials, some of them, such as carbamazepine (CBZ) cocrystals, exhibit a channel-like structure in which the coformer molecules such as tartaric, maleic, malonic or oxalic acids are disordered inside the channels.[47,48] To the authors' knowledge, the exact nature of this disorder (partial, total, translational, orientational, static or dynamic) has not been investigated yet. Despite their disordered nature, coformer molecules inside the channels are intrinsically part of the overall crystal and they do not leave the channels. These cocrystalline systems should thus not be confused with inclusion compounds or crystals with solvent inclusion in which the crystalline structure can also be made of channels filled with disordered molecules but for which the content can significantly vary.[49,50]

For example, the pure carbamazepine form II shows a hydrophobic channel-like structure which may (or not) contain various type of disordered solvent molecules such as tetrahydrofuran,[51] n-tridecane[49] or toluene[49] used for crystallization of this form. It has been

shown that the presence of these solvent molecules contributes to stabilization of the crystal structure. However, only weak interactions between solvent molecules and the hydrophobic aromatic surfaces of the channels were suspected and such a stabilization would just originate from the filling of the voids in the structure. Solvent loss can be detected easily upon specific drying or heating procedures[48,49,51] depending in particular on the size of the solvent molecules. An isostructural crystal of form II of carbamazepine has been also obtained in which some disordered hydrogen bonded water wires are encapsulated inside the channels.[52]

In this study, we analyze in detail the exact nature of the disorder of the tartaric acid (TA) molecules in the CBZ:TA cocrystal assembled by liquid assisted grinding. Experimentally, the cocrystal was obtained using the pure isomer L-tartaric acid (Figure 1.a). The active pharmaceutical ingredient carbamazepine (Figure 1.a) creates a channel-like architecture, where dimers of CBZ molecules are stacked to each other in such a way that form unidimensional hydrophilic channels of about 1 nm size (Figure 1.b). These channels are filled with tartaric acid in a disordered state. The investigations are based on complementary Broadband Dielectric Spectroscopy (BDS), Powder X-ray Diffraction (PXRD) and ^{1}H-^{13}C CP/MAS solid-state NMR (ss-NMR) experiments combined with MD simulations. The synergistic combination of these studies provides a thorough analysis of the structural organization, the intermolecular hydrogen bonding interactions, the rotational and translational dynamics of the TA molecules in the CBZ channels.

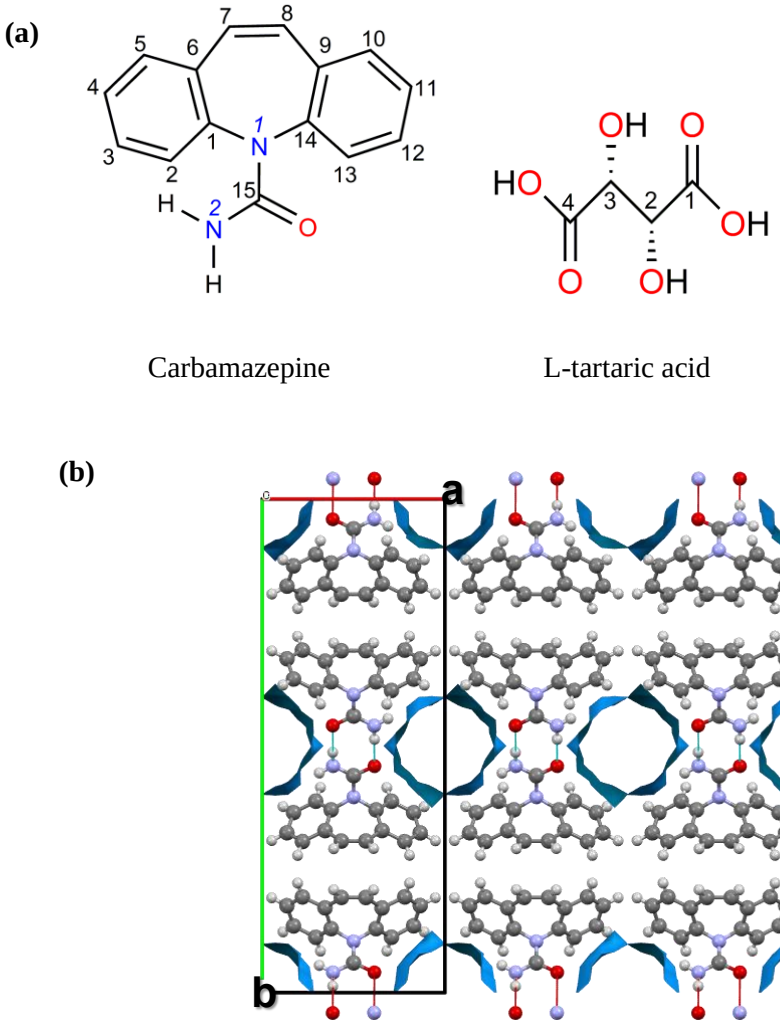

Figure 1. (a) Molecular structures of carbamazepine (CBZ) and L-tartaric acid. (b) Projection of the unit cell along the [001] direction of the channel-like structure CBZ based cocrystal (monoclinic, space group $P2_1/c$, CSD Refcode MOXWIG). The hydrophilic channels formed by the CBZ molecules in the structures are illustrated in blue (empty channels). The diameter of one channel is about 1 nm.

RESULTS AND DISCUSSION

Structure and intermolecular hydrogen bond interactions

The CBZ:TA cocrystal, that was synthetized by Childs *et al.*,[53] shows a channel-like architecture,[47] where dimers of carbamazepine molecules are stacked to each other in such a way that it forms hydrophilic channels of nanometer size (Figure 1.b), which are filled with disordered tartaric acid molecules. The cocrystal described by Childs *et al.*[47] was obtained using DL-tartaric acid as the cocrystal coformer. Nevertheless, DL-tartaric acid and L-tartaric

acid give similar X-ray diffractograms (data not shown), thus, and for simplicity, the investigation in this paper was performed using L-tartaric acid, hereinafter referred to as TA. In the cocrystalline structure of the channel-like CBZ:TA cocrystal, the position of the coformer TA molecules in the channels has not been solved due to the high disorder[47] and, in addition, the exact stoichiometry was actually not determined.[53]

In order to obtain more information on the nature of the disorder of the TA molecules into the CBZ nanometric channels, ^{1}H-^{13}C CP/MAS solid-state NMR (ss-NMR) measurements have been performed. The spectra of the CBZ:TA cocrystal as well as those for CBZ (form III) and TA parent compounds are shown in Figure 2. According to the literature,[54] the two doublet resonances observed in the ^{13}C CP/MAS NMR spectrum (Figure 2.a) of the L-tartaric acid crystal (monoclinic, space group $P2_1$, two molecules in the unit cell)[55] reflect the non-equivalence of the two carboxylic and the two α-carbon atoms (Figure 1.a) due to the four different types of hydrogen bonds between adjacent molecules that constitute the hydrogen-bonded networks of the TA crystalline structure.[55] The peaks at 176.7 and 172.2 ppm are assigned[54] to the carboxylic ^{13}C sites (C1 and C4) and the resonances at 74.7 ppm and 72.7 ppm to the α-carbons (C3 and C2) (see Figure 1.a). Figure 2.a shows that the resonance at 74.7 ppm is no longer present in the cocrystal, which is a strong indication that TA has been completely co-crystallized. However, the resonance at 72.7 ppm remains after cocrystallization which indicates that some order could persist. The carboxylic carbons are represented by a considerably broadened lines in the range of 176.7 and 172.2 ppm almost disappeared giving rise to a broad and very weak resonance indicating conformational site disorder affecting the TA molecules. This result corroborates the presence of disorder suggested by PXRD analysis.[47] The CBZ:TA cocrystal also exhibits a peak at 159 ppm attributed[56] to the carbonyl carbon (C15) of the amide group of CBZ (see Figure 1.a). Figure 2.b shows the ^{1}H-^{13}C CP/MAS NMR spectrum in the range 145-120 ppm, where only characteristic CBZ signals appear (overlapping

aromatic and ethylenic carbon signals).[56] The resonances observed at 137.09 and 140.42 ppm in the CBZ form III (P-monoclinic, space group $P2_1/c$)[57] correspond to the carbon sites C1 and C14 respectively (see Figure 1.a), *i.e.*, the carbon (C1) near to the NH_2 group of the amide moiety and the carbon (C14) near to the carbonyl oxygen atom.[56] It should be noted that only a single broad signal at 140 ppm (due to a combined contribution from C1/C14 sites) is observed in the CBZ:TA cocrystal. It might be suggested that both $–NH_2$ and C=O groups of the CBZ molecules in the vicinity of the C1 and C14 sites in CBZ could be affected by the presence of the disordered TA molecules. One may possibly find hydrogen bonds between the TA and the CBZ molecules as it will be seen by the MD simulations below. This possibility is also suggested in results[48] for other CBZ based cocrystals filled with disordered small molecules capable of forming hydrogen bonds.

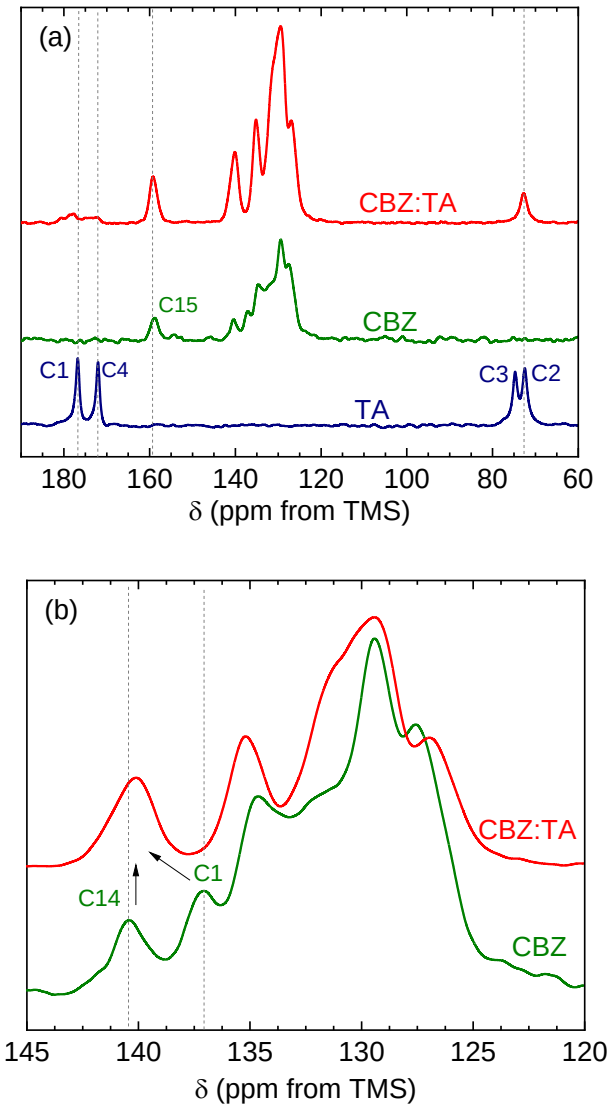

Figure 2. ^{1}H-^{13}C CP/MAS solid-state NMR spectra of the cocrystal CBZ:TA (red line at the top) in comparison with pure parent compounds, carbamazepine form III, CBZ and L-tartaric acid, TA (olive and navy lines at the bottom). All spectra were acquired at 298 K using MAS rates of 10 kHz (a) and (b) Aromatic and ethylenic region of CBZ and CBZ/TA spectra. See Figure 1.a (molecular structures with carbon numbering) and text for details for peak assignment.

In order to get a deeper insight into structural organization in the CBZ:TA cocrystal, we compared PXRD patterns of the pure parent compounds CBZ form III[57] and TA[58] used to design this cocrystal (Figure 3.a) and the CBZ:TA cocrystal itself obtained in the present study (Figure 3.b). The calculated PXRD pattern of the structure proposed by Childs *et al.*,[47] *i.e.* without the TA molecules, is also represented in Figure 3.c. The diffractogram of the CBZ:TA cocrystal significantly differs from the PXRD pattern of the pure parent compounds and

matches well with the structure proposed by Childs *et al.*[47] This resemblance between the two can be particularly observed at low-angle Bragg peaks at $2\theta \approx 6.5°$, 8.8° and 13.1° (corresponding to the Miller planes (020), (120) and (040)[47]), which are typical of the channel-type architecture of the CBZ host framework (Figure 1.b and Figure 3.c). However, one may note a discrepancy between the diffractogram of the CBZ:TA cocrystal and the calculated PXRD pattern based on the structure proposed Childs *et al.*[47] Indeed, quite an intense Bragg's peak at $2\theta \approx 15.8°$ is found experimentally for the CBZ:TA (see Figure 3.b) while it is almost absent from the calculated diffractogram (see Figure 3.c). Nevertheless, a zoom of the calculated PXRD pattern around $2\theta \approx 15.8°$ allows us to observe this peak but it exhibits an extremely weak intensity (see Figure S1). This peak at $2\theta \approx 15.8°$, corresponding to a Miller plane (140), has indeed been indexed in the resolution of the structure performed by Childs *et al.*,[47] but the intensity clearly does not correspond to the intensity obtained from the experimental cocrystal (whether in this work or in the experimental result of Childs *et al.*[53]).

Since the calculated PXRD pattern (Figure 3.c) is based on a structure not including the TA molecules, one might assume that the intense Bragg peak at $2\theta \approx 15.8°$ (Figure 3.b) could originate from the presence of the TA molecules in the hydrophilic CBZ channels.

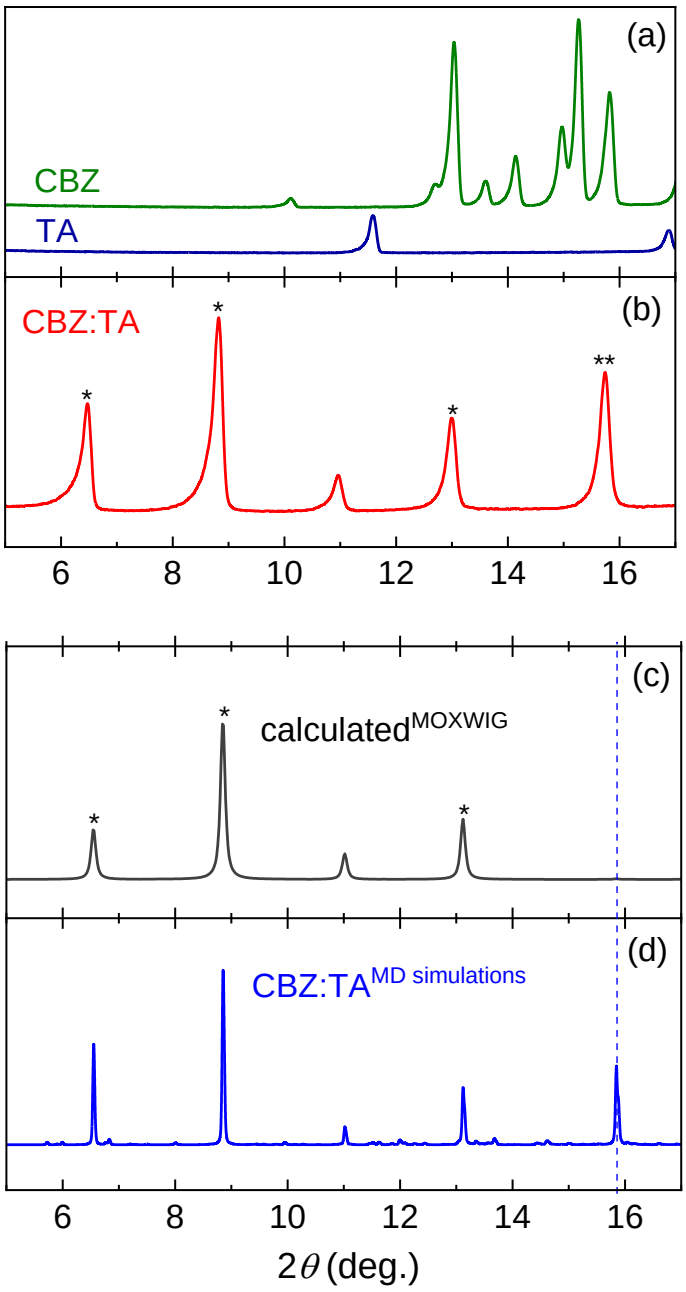

Figure 3. (a) PXRD patterns (at 298 K) of the pure parent compounds CBZ (Form III)[57] and L-tartaric acid (TA),[58] (b) PXRD pattern (at 298 K) of cocrystal CBZ:TA, (c) PXRD pattern calculated according to the literature (CSD Refcode MOXWIG). This PXRD pattern does not take into account the TA molecules in the channels since their atomic positions were not determined due to their high disorder and (d) PXRD pattern calculated based on MD simulations results of the CBZ:TA cocrystal in which the channel architecture MOXWIG is used for the CBZ molecules. The peaks labelled by one asterisk ($2\theta \approx 6.5°$, 8.8° and 13.1°) represent the characteristic peaks of CBZ channel structure in the cocrystal.[47] The peak labelled with two asterisks ($2\theta \approx 15.8°$) represents a characteristic peak associated to the TA molecules inside the CBZ channel-like structure as shown by MD simulations (see text).

In order to shed light on the structural organization of the TA molecules in the CBZ nanometric channels, MD simulations have been performed (see details in section materials & methods). The CBZ:TA cocrystal model was constructed based on the structure proposed by Childs *et al*.[47] in which the channels were filled with TA molecules with random positions following the (3:1) stoichiometry established by LAG experiments.[59] This initial structure was then heated and equilibrated at high temperatures at 530 K and above at constant pressure in order to allow the TA molecules to reorganize and adopt stable positions and orientations compatible with the presence of the CBZ molecules forming the channel-like structure. Some snapshots of the CBZ:TA cocrystal model are displayed in Figure 4.a and Figure 4.b. In Figure 4.b, one can notice that the channel is not completely filled. TA molecules are distributed in small groups of molecules separated by some "empty spaces". In order of facilitate the comparison with the experimental data obtained from X-ray diffraction, we have also performed MD simulations by fixing the atomic positions of the CBZ molecules at their experimental values corresponding to the structure proposed by Childs *et al*..[47] These structures were then also heated at 530 K and above but only at constant volume in this case. Subsequently, these structures were also optimized using a conjugated gradient algorithm. A snapshot of the optimized structure is displayed in Figure 4.c. In order to confirm the assumption made on the origin of the intense Bragg peak at $2\theta \approx 15.8°$, we have calculated the PXRD pattern based on the optimized structure obtained from MD simulations which includes both CBZ and TA molecules, as represented in Figure 3.d. As expected, since the atomic positions of CBZ molecules have been kept to the Childs *et al*.[47] structure (Figure 3.c), Bragg peaks perfectly match. However, the intense Bragg peak at $2\theta \approx 15.8°$ observed experimentally is also well reproduced confirming its origin linked to the presence of the TA molecules.

This peak $2\theta \approx 15.8°$ corresponds to a Miller plane (140) as indexed by Childs *et al.*,[47] and thus to planes parallel to the crystallographic $\vec{c}$ axis. Based on the PXRD and indexation, no

clear peak seems associated to some structural organization along the crystallographic $\vec{c}$ axis. Interestingly, the snapshot of the CBZ:TA cocrystal optimized structure displayed in Figure 4.c suggests that the TA molecules are actually less disordered than previously hypothesized by Childs *et al.*[47] and form a sort of bridge through hydrogen bonds (HB) between two adjacent CBZ molecules along the direction of the channel. Indeed, by computing the HBs formed between TA and CBZ molecules (see details in section materials & methods), one finds that the hydroxyl group –OH belonging to the carboxylic groups of the TA molecules are hydrogen bonded to the carbonyl C=O of the carboxamide group of the CBZ molecules. It thus highlights some periodicity for the atomic positions of the TA especially for the carboxylic groups which does not seem to be detectable by PXRD.

In order to support this idea, we have calculated the axial density distribution profiles along the channel direction of the oxygen atom belonging to the carboxamide C=O group of the CBZ molecules and the oxygen atom belonging to the –OH group of the carboxylic groups of the TA molecules at a relatively high temperature T = 530 K (figure 5.a). As a whole, both profiles display very similar trends of correlated periodical alternations due to the long range periodicity along the direction of the channel. Therefore, this figure clearly confirms the correlation between the position of the oxygen atoms belonging to both CBZ and TA molecules due to the formation of HBs. In Figure 5.b, the pair distribution function (PDF) of the center of mass of the TA molecules has been also calculated along the channels. It confirms the partial ordering of the TA molecules and the organization of the molecules which can be described as file of TA molecules along the channel. The average distance between the center of mass of neighboring TA molecules is about 6.5 to 7 Å and does not seem to be dependent of the temperature.

A thorough analysis of the intermolecular HB associations that can be formed between the different TA and CBZ molecules in the cocrystal has been also performed. The TA molecule

possesses four –OH hydroxyl groups and two C=O groups while the CBZ molecule possesses one amide group, $–NH_2CO$ (see Figure 1.a). The –OH and –NH moieties can participate to HB, either as H-donor or as H-acceptor while the C=O group can only be H-acceptor. Many HBs can thus potentially be formed in the system. It should be noted that CBZ molecules form a cyclic dimer in the crystal at the origin of the channel-like structure (see Figure 1.b and Figure 4.a). In order to identify HBs, a geometric criterion has been chosen as follows: two molecules are considered to be H-bonded if *i)* the nitrogen-oxygen or the oxygen-oxygen distance is less than 3.4 Å and *ii)* the (N···H-O) or (O···H-O) angle is larger than 150°. This criterion is in some way arbitrary due to the lack of information on the electron density but it has been successfully used in many MD simulations and allows us to take into account relatively well formed HBs in statistics.[60,61] Based on this criterion, no HB is found between the –NH moiety of the CBZ molecules and the C=O and –OH groups of the TA molecules. It should be mentioned that the use of a less strict criterion for the definition of the HB indicates that some very deformed HB can possibly exist between the –NH moiety of the CBZ molecules and the C=O and –OH groups of the TA molecules but they have not been investigated in the present study. Oppositely, a large number of very well formed HBs are found between the C=O group of the CBZ molecules and the four –OH hydroxyl groups of the TA molecules. Detailed results are reported in Table 1. For the optimized structure, data show that *ca.* 85% of all –OH of the TA carboxylic groups form one relatively well-formed HB with the C=O group of the CBZ molecules, which is consistent with the snapshot displayed in Figure 4.c. One may note that *ca*. 40% of the lateral –OH group of the TA molecule also form this type of well-formed HB but to a less extend. These features confirm the expected strong HB affinity between the TA molecules and the CBZ hydrophilic channel. Table 1 clearly also suggests that this HB affinity persists even at very high temperatures (T = 530 K). An analysis has been also performed for the HB associations between TA belonging to the same channel (Figure 4.b). Some HBs can

be actually formed between TA molecules but their number remain relatively small compared to the number HBs formed between TA and CBZ molecules. Some examples of such TA...TA HBs are displayed in the Figure 4.b and Figure 4.c. It is highlighted in the snapshot displayed in Figure 4.b that the channels of the structure are actually not completely filled and some "empty spaces" can exist in between some of TA molecules, which limit the possibility to form HBs. The statistics of chains formed by the TA molecules and separated by "empty spaces" will be analyzed in the following section devoted to translational dynamics. It should be mentioned that the results obtained in the present study are in good agreement with the conclusions of a recent publication comparing the nature of the intermolecular interactions of other small molecules in channels made of CBZ molecules.[48] We will see in the next sections that the organization of the TA molecules is not static. TA molecules experience rotational and translational diffusion and HBs can thus break and reform.

It could be reasonably assumed that such many HB bridges formed by TA molecules between adjacent CBZ molecules along the channel direction (see Figure 4.c) could certainly contribute to the stability of the CBZ:TA cocrystal. It could particularly explain the origin of the (3:1) stoichiometry found in the stoichiometry screening[59] made for this cocrystal. Indeed, a smaller number of TA molecules would decrease the number of TA and CBZ bridges, which would decrease the stability. A higher number of TA molecules would certainly help to fill the "empty spaces" mentioned above but would also increase the number of HBs between TA molecules. However, the highest propensity of HBs between TA molecules could also decrease the number of HB bridges formed by TA molecules between adjacent CBZ molecules along the channel direction and could thus also destabilize the overall structure.

Table 1. Fraction of –OH groups of the TA molecules forming HB with the C=O group of the CBZ molecules (see molecular structures in Figure 1.a). –OH (lateral) refers to the hydroxyl groups bonded to carbon 2 and 3 in Figure 1a while –OH (carboxylic) to the hydroxyl group of the carboxylic group (carbon 1 and 4 in Figure 1.a).

	T = 530 K	**Optimized structure** **T = 0 K**
–OH (lateral)	26 ± 2 %	40 ± 2%
–OH (carboxylic)	58 ± 2 %	85 ± 2 %

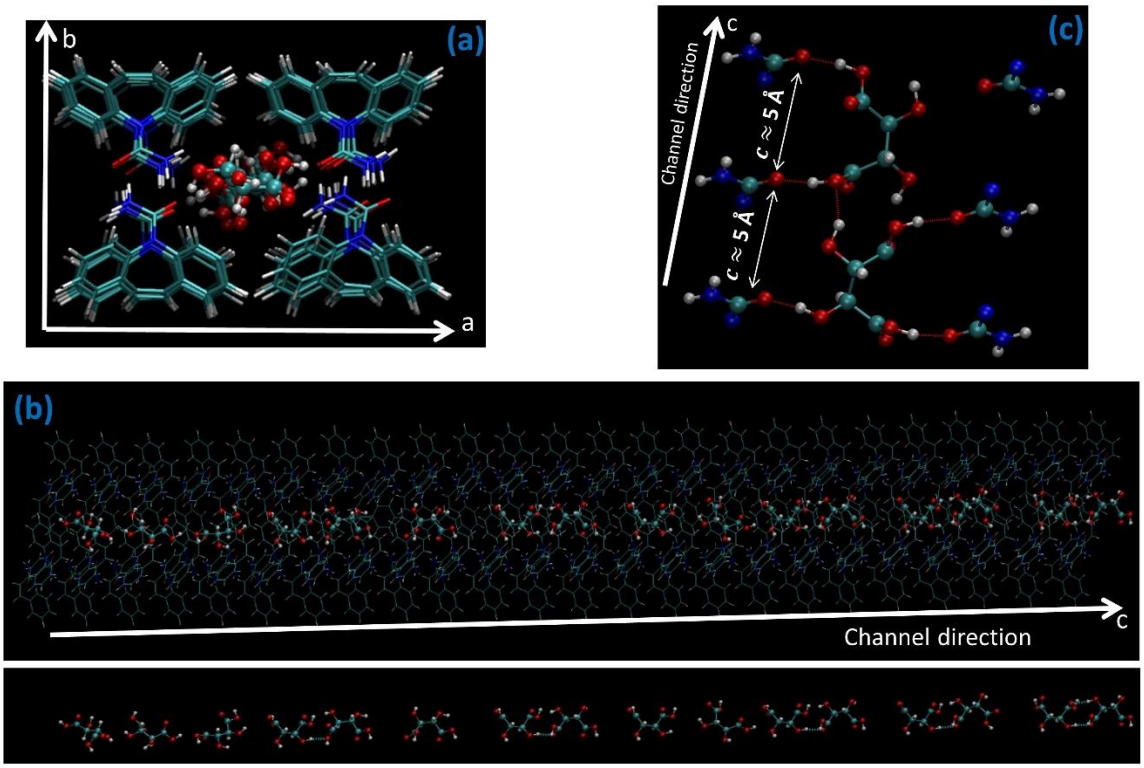

Figure 4. Snapshots of structures of the CBZ:TA cocrystal obtained from MD simulations. (a) One channel made of CBZ molecules and filled with TA molecules at T = 530 K. It is a projection in the $(\vec{a}, \vec{b})$ crystallographic plane of the structure, (b) Example of one CBZ channel filled with TA molecules along the $\vec{c}$ crystallographic direction at T = 530 K. At the bottom, the same snapshot is provided without the CBZ molecules for clarity and in order to show that the channel is not completely filled with TA molecules. TA molecules are organized in small groups or molecules separated by some empty spaces of about 5 Å. The total length of this channel is about 126 Å (see section materials & methods) and (c) One local optimized structure (T = 0 K) showing the interactions between two TA molecules and the CBZ channel structure. For clarity, only the carboxamide functional group of the CBZ molecules are represented. Hydrogen bonds are represented by dotted lines. The distance between two adjacent C=O groups along the channel direction correspond to the crystal cell parameter $c \approx 5$ Å.

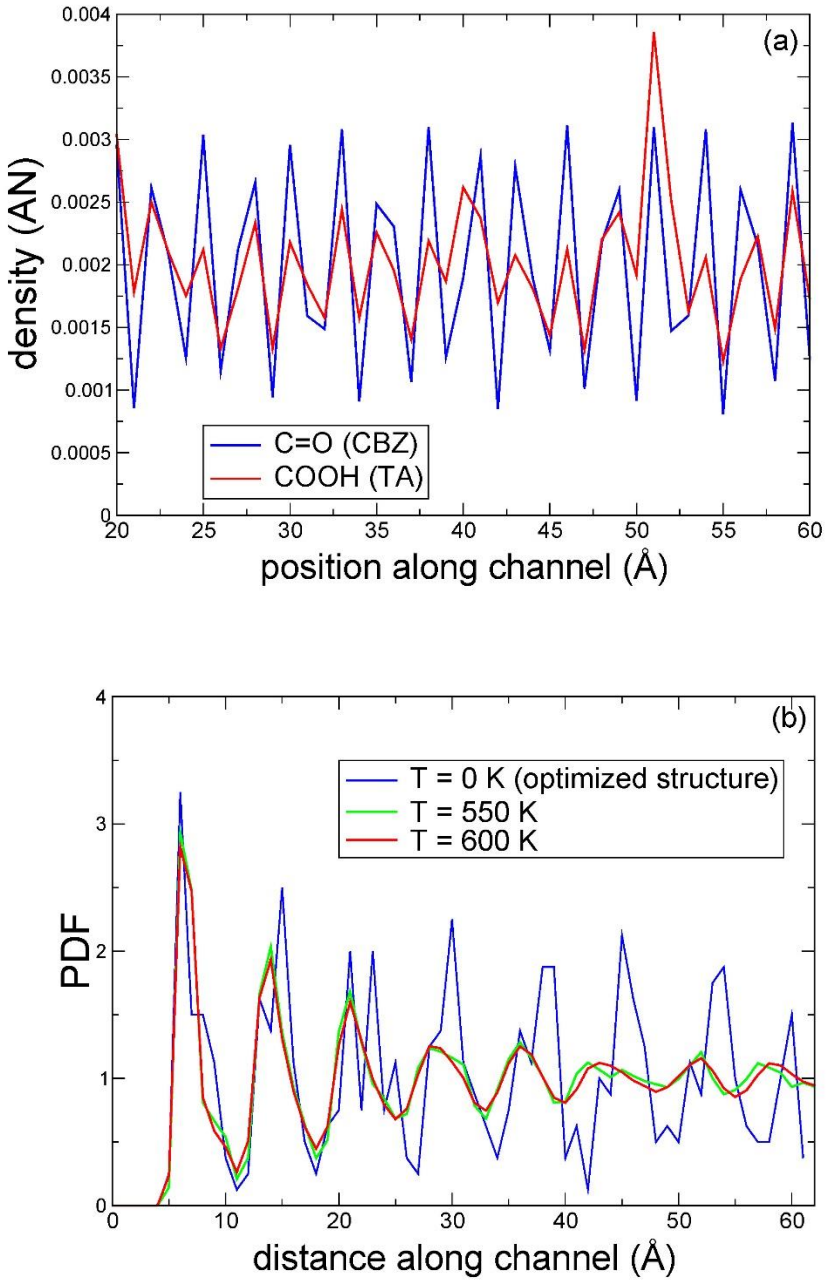

Figure 5. MD simulation results. (a) Axial density distribution profiles along the channel direction of the oxygen atom belonging to the carboxamide group of the CBZ molecules (C=O) and the oxygen atom belonging to the –OH of the carboxylic groups of the TA molecules (COOH) obtained at T = 530 K. The axial density along the channel is only represented between 20 and 60 Å for clarity but it presents the same features all along the channel long of 130 Å and (b) Pair distribution function (PDF) of the center of mass of the TA molecules along the channel direction. PDF has been separately calculated for each channel then averaged over all channels. PDF is represented at 0 K (optimized structure), 550 K and 600 K. The signal is relatively noisy for the optimized structure since only one configuration is used for the PDF computations.

Rotational dynamics

PXRD, ss-NMR and MD simulations results indicate some partial disordered state for the TA molecules in the CBZ:TA cocrystal at room temperature. This disorder can be either static or dynamic in nature. Taking advantage of the fact that the TA is a polar molecule with a dipole moment $\mu = 2.8$ Debye computed from Gaussian using the HF/6-31G* basis set,[63] we used here dielectric spectroscopy to study molecular mobility. It is probed through the reorientations of dipoles under an alternating electric field of frequency (ν) varying from 0.1 Hz to 10 MHz, in the temperature range from 143 to 373 K.

Figure 6.a and Figure 6.b show the imaginary part (dielectric loss) of the complex permittivity ($\varepsilon^*(\nu) = \varepsilon'(\nu)\text{-}i\varepsilon''(\nu)$) at representative temperatures, $\varepsilon''(\nu)$, and frequencies, $\varepsilon''(T)$, respectively. The well-defined peaks (and the step-like decrease seen in $\varepsilon'(\nu)$ shown in Figure S2.a), which continuously shift to higher frequencies with increasing temperature, are typical features of thermally activated relaxation modes. These modes are found in many disordered materials,[64,65] including crystalline systems like orientationally disordered (or plastic) crystals[66-68] that are molecular crystals in which the molecular centers of mass form a regular crystal, while some dynamical disorder exists in the molecular orientations.[69,70] The dielectric behavior of the CBZ:TA cocrystal is completely different from that of the parent crystalline compounds (Figure 6.c). In the same frequency and temperature ranges, the dielectric loss spectra of CBZ and TA are featureless, as expected for the dielectric response from a fully ordered crystalline state where the dipoles are insensitive to electric fluctuations in the covered frequency range. In this way, we have clearly demonstrated for the first time the dynamic nature of the disorder of TA molecules in the CBZ:TA cocrystalline system.

The dielectric loss spectra of the CBZ:TA cocrystal exhibit two relaxation features (Figure 6.a and Figure 6.b), a more intense one that we have called as “I-process” and a less intense one at

high frequencies (faster) on the right flank of the slower I-relaxation, labeled as "II-process". At temperatures above *ca.* 273 K, another process shows up as an increase of ε″ and ε′ in the low frequency region of the spectra (Figure S2.b), which can be attributed to an interfacial Maxwell−Wagner-Sillars (MWS)[8] process arising from the heterogeneous nature of the multicomponent system. It will be investigated in detail in a separate study. Here, we mainly focus on the behavior of the I- and II-relaxation processes. Solid lines in Figure 6.a are fits to the spectra using a sum of two symmetric Cole-Cole (CC)[64,71] functions (equation (1) in Materials and Methods), as illustrated for the spectrum acquired at 233 K (dashed lines). The width (measured by the β_{CC} parameter) of the I-relaxation has been found to be almost constant in all temperature range ($\beta_{CC,I}$ = 0.86) while the II-process becomes narrower with increasing temperature ($\beta_{CC,II}$ varies from 0.4 (233 K) to 0.7 (313 K). Such deviations from the Debye behavior (β_{CC} = 1 for non-interacting dipoles) indicate a distribution of relaxation times (the smaller the β_{CC} values, the wider the distribution of relaxation times), usual in disordered systems,[8] including orientationally disordered crystals.[66] We also analyzed the representation of ε″ *versus* temperature at constant frequencies (isochronal plot) using a sum of two Gaussians (dashed lines in Figure 6.b) to obtain the maximum temperature of peaks, T_{max}, for each measured frequency.

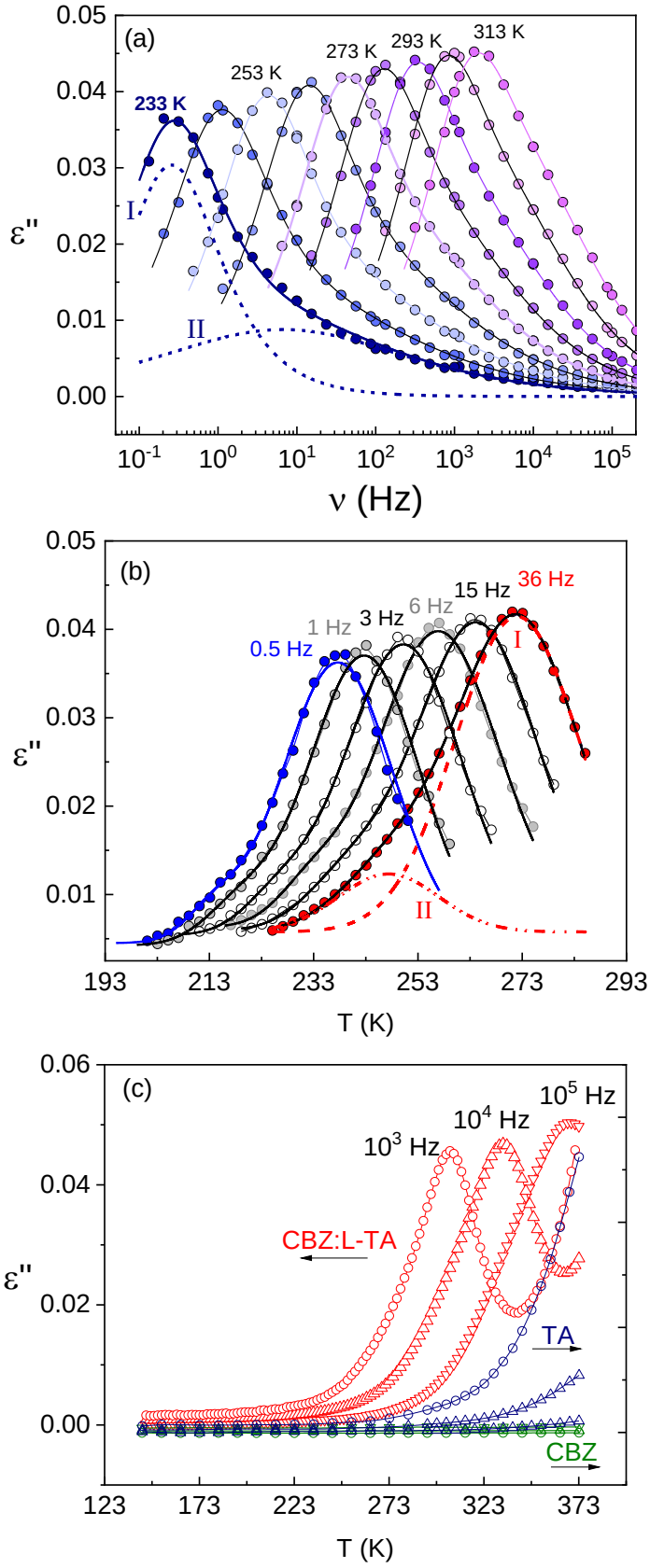

Figure 6. (a) Dielectric loss spectra (ε′′(ν)) of CBZ:TA cocrystal for selected temperatures (from 233 K to 313 K, steps of 10°). Solid lines are fits to the experimental data using a sum of two Cole-Cole (equation 1) functions as illustrated for ε′′(ν) spectrum obtained at 233 K (royal dashed lines; processes I and II). (b) Isochronal representation, ε′′(T), at selected frequencies (ν) (data

taken from isothermal measurements). Solid lines are the global fit using a sum of two Gaussian functions (illustrated for ε′′(T) at 36 Hz; red dashed lines). (c) Comparison of ε′′(T) of CBZ:TA cocrystal (red symbols; left-hand vertical axis) with TA (navy symbols) and CBZ (olive symbols; right-hand axis in *a.u.*), at indicated frequencies.

Figure 7 shows the temperature dependence of relaxation times (τ) obtained from the two analyses of dielectric data: isothermal, τ_{CC} (the most probable relaxation time related to the frequency of $\varepsilon''(\nu)$ maximum, $\tau_{CC} = 1/(2\pi\nu_{max})$) and isochronal, τ ($\tau = 1/(2\pi\nu)$, at which $\varepsilon''(T)$ presents a peak at T_{max}), that are in good agreement with each other. Both processes follow an Arrhenius-like temperature dependence, $\tau(T) = \tau_\infty exp(E_a/RT)$ (where E_a is an energy barrier and τ_∞, the pre-exponential factor, is the limiting relaxation time at high temperature and R is the universal gas constant), in the whole temperature range investigated. The Arrhenius parameters calculated from the straight lines through the data points are $E_{a,I}$ = 67 kJ·mol^{-1}, $\tau_{\infty,I}$ = 8×10^{-16} s and $E_{a,II}$ = 58 kJ·mol^{-1}, $\tau_{\infty,II}$ = 2×10^{-15} s, for the I- and II-relaxation, respectively. The Arrhenius pre-exponential factor values are a little lower than expected from the inverse of a vibrational attempt angular frequency (*ca.* 10^{13}–10^{14} Hz). The use of the Eyring formalism to describe the temperature dependence of the relaxation time, and the established relationships with the Arrhenius parameters,[72] allow us to propose a physically reasonable interpretation in order to attempt to assign their molecular origin. The II-relaxation width was found to decrease with increasing temperature (increasing $\beta_{CC,II}$), indicating a distribution of processes composing it. The linear temperature dependence of the most probable relaxation time $\tau_{II}(T)$ can be rationalized by assuming the II-relaxation to be distributed in energy, but not in the pre-exponential factor (*i.e.*, with no entropic contribution): $\tau_{II}(T) = 10^{-13}exp[(58000 - 32.5T)/RT]$, where the most probable activation energy slightly decreases with increasing temperature ($E_{a,II} = 58000 + aT$ with a = -32.5 J·mol^{-1}·K^{-1}). For the I-relaxation, temperature affects the most probable time without modifying the profile of

the frequency-dependent dielectric loss peak ($\beta_{CC,I}$ constant). The Arrhenius pre-exponential factor value could reflect a non-zero and constant entropic contribution ($\Delta^{\ddagger}S°$ = 35 J·K^{-1}·mol^{-1}): $\tau_I(T) = \left[10^{-13.3} exp\left(-\frac{35}{R}\right)\right] exp\left(\frac{64000}{RT}\right)$, where $\Delta^{\ddagger}H°$ = 64 kJ·mol^{-1} ($\cong E_{a,I}$) is the associated constant activation enthalpy. This slight molecular cooperativity points to an intermolecular origin of the I-relaxation. As shown in Figure 7, the extrapolated lines of $\tau_{II}(T)$ and $\tau_I(T)$ merge at high temperature when $\tau_I = \tau_{II} \sim 10^{-12}$ s, indicating a correlation between I- and the II-relaxation. The cyan lozenges in Figure 7, that coincide with experimental τ_{II}(T), are the primitive (one-body, non-cooperative) relaxation times, τ_0(T), calculated by applying the Coupling Model (CM) equation,[73,74] $\tau_0(T) = (t_c)^n \tau_I(T)^{1-n}$, where $(1-n) \equiv \beta_{KWW}$ is the fractional exponential of the Kohlrausch–Williams–Watts (KWW) stretched correlation function, $\phi(t) = exp\left[-(t/\tau_{KWW})^{\beta_{KWW}}\right]$,[75–77] describing the many-body (cooperative) I-relaxation in the time domain (β_{KWW} = 0.88 using the approximation[78] $\beta_{KWW} \approx (\beta_{CC})^{1/1.23}$). In the CM context, the onset of cooperativity due to intermolecular coupling occurs at t_c, a constant crossover time ($t_c \approx$ 1-2 ps).[74] In addition to the coincidence of τ_{II}(T) with predicted τ_0(T) values, the activation energies of the observed processes verify well the relationship $E_{a,II} = E_{a,I}(1-n)$ predicted by the CM,[74] strengthening their correlation. Therefore, the II-relaxation found here for the dynamically disordered TA molecules in the channels of the CBZ rigid matrix could be considered to be of intermolecular origin and, the (non-cooperative) precursor of the I-relaxation (slightly cooperative).

For many molecular compounds,[74] the freezing of the dipolar molecular motions in the dielectric measurement timescale (*ca.* 100 s – 1000 s) is associated to the well-known glass transition phenomenon in which an equilibrium liquid is transformed to a nonequilibrium disordered solid. This transformation is also evidenced from thermodynamic properties, such as the heat capacity or thermal expansivity.[79] Interestingly, the glass transition phenomenon is

also observed in rotationally disordered crystals or plastic crystals such as for example caffeine.[67]

For the CBZ:TA cocrystal (disordered), no calorimetric signature is detected by DSC (see thermogram in Figure S3) in the temperature ranges at which the dipolar molecular motions reach ~100 s – 1000 s in the dielectric measurements. However, glass-forming materials which exhibit molecular mobility having a very pronounced Arrhenius-like temperature dependence, *i.e*. the so-called strong glass-formers, usually show a barely detectable heat capacity Cp-jump characteristic by DSC.[80,81] It is for example the case for caffeine.[67] In contrast, while no change in the overall structure of the cocrystal is observed (Figure S4), the temperature dependence of the cell volume (V(T)) shows a clear kink at *ca*. 173 K (see inset in Figure 7 and Figure S5). Interestingly, this temperature corresponds very well to the temperature at which the freezing of molecular motions associated with II-process occurs ($\tau_{II} = 10^3$ s, extrapolated dashed line in Figure 7, at $-\log(\tau_{II}(s)) = -3$) suggesting that they provide information about the local environment of disordered TA (guest) molecules in the CBZ rigid (host) matrix. It is well in line with the intermolecular HB interactions between TA and CBZ molecules shown by MD simulations (see Figure 4.c and Table 1). For the I-relaxation process, one finds $\tau_I = 10^3$ s at about a temperature of 193 K by extrapolation (see inset in Figure 7) which is also close to the temperature at which the kink in V(T) trace is detected. Thus, it reinforces the possible link suggested between both I- and II- processes. These results suggest that the statistical disorder observed by PXRD which is largely dynamic above $T_{II}(\tau_{II} = 10^3 \text{ s}) = 173$ K becomes static below this temperature, where the low amplitude II-relaxation is kinetically frozen. The small change in the degree of crystal anharmonicity (or molecular mobility amplitude) in the temperatures range at which the kink is detected is also in agreement with the absence of a heat capacity signal.

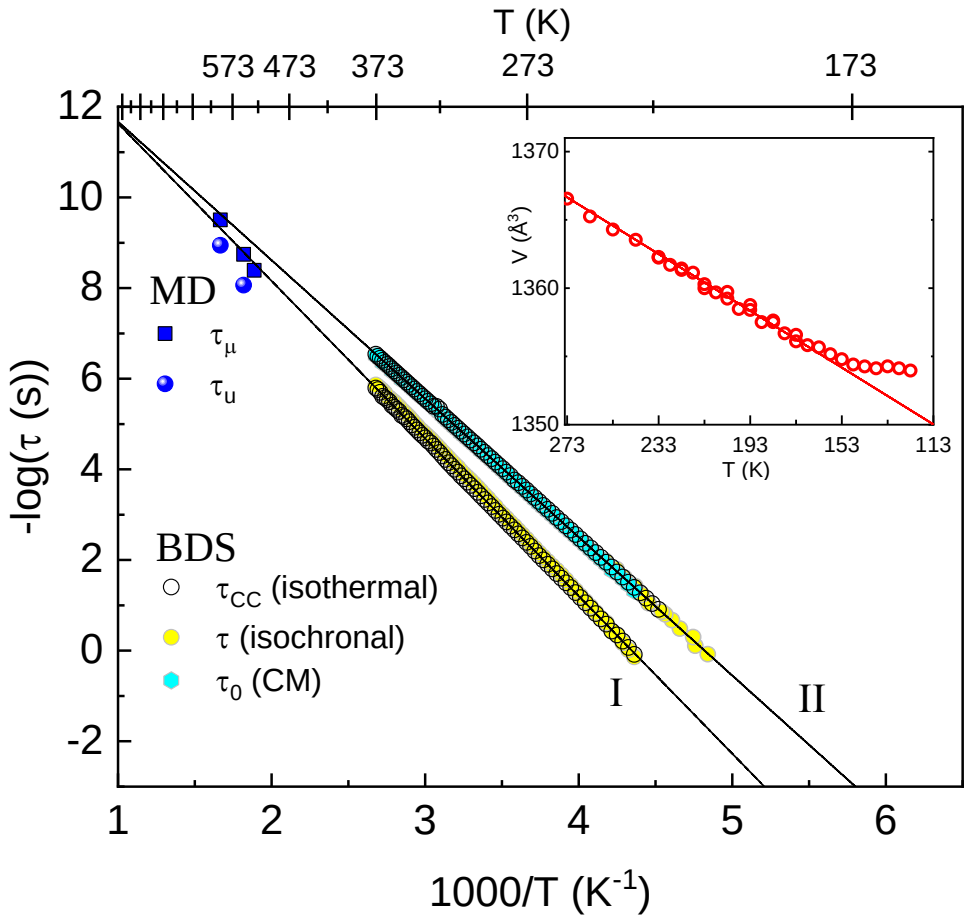

Figure 7. Temperature dependence of the I- and II-relaxation times obtained from fits of isothermal, τ_{CC} (open circles) and isochronal dielectric data, τ (yellow filled circles) in an Arrhenius representation ($-\log_{10}(\tau)$ *versus* 1/T). The solid lines are the fits with the Arrhenius law. Cyan lozenges are the relaxation times predicted from Coupling model, τ_0 (CM). Blue squares and spheres are times obtained from molecular dynamics (MD) simulations. See text for details. The temperature evolution of the volume of the crystalline cell of the CBZ:TA cocrystal is represented in inset (Figure S5 shows V(T) from 123 K to 373 K).

The molecular mobility in the disordered CBZ:TA cocrystal revealed by BDS experiments has been also confirmed by MD simulations. Molecular reorientations have been probed at high temperatures at 530, 550 and 600 K in the pico- nano-second time range accessible by the MD simulations. Two descriptors were used to describe orientations: the vector $\vec{u}$ orientated along the central C-C bond of the TA molecules (see inset in Figure 8) as well as the dipole moments $\vec{\mu}$ of these molecules.[82] The dipole moments $\vec{\mu}$ cannot be easily represented because its orientation is strongly dependent of the conformations of the TA molecules, which vary

significantly. Indeed, the TA molecule possesses a very high flexibility that can be demonstrated by the very broad distribution of the dipole moment $\|\vec{\mu}\|$ (see Figure S6). In Figure 8.a, the distribution of the TA molecules orientations in the channels is represented based on the vector $\vec{u}$. This figure shows that the TA molecules actually adopt two preferential orientations by forming an angle of about $\theta_u \approx 30°$ or 150° with the direction of the channels (see inset in Figure 8.a). This result is consistent with the local optimized structure (T = 0 K) displayed in Figure 4.c related to the interactions between TA molecules and the CBZ channel structure. The time evolution of the orientation of one targeted TA molecule is plotted in Figure 8.b. It reveals that the orientation of the molecules is not fixed and several jumps between the preferable orientations (30° and 150°) are clearly observed over the duration of the simulation. This last result nicely confirms that the TA molecules are partially ordered in the channels as shown in the previous section (see for example Figures 2, 3d, 4c and 5) but also present molecular mobility. In Figure 9, the time-dependent self-correlation function $\Phi_u(t) = \langle \vec{u}(t).\vec{u}(0) \rangle$ and $\Phi_\mu(t) = \langle \vec{\mu}(t).\vec{\mu}(0) \rangle$ have been represented for the two orientational descriptors.[82] The symbol $\langle \quad \rangle$ indicates an average over both time and molecules. Figure 9 confirms that TA molecules are actually rotating and allows extracting some additional information, in particular, the times characterizing the rotational dynamics. The long-time behavior of the $\Phi_u(t)$ and $\Phi_\mu(t)$ functions can be fitted by a stretched exponential function $ae^{-(t/\tau)^\beta}$ where a, τ and β are the fitting parameters. In a first approximation, the complex frequency dependent permittivity ε*(ν) measured experimentally by BDS is actually roughly proportional to the Fourier transform of the time-dependent correlation function of the dipole moment $\Phi_\mu(t)$.[83] The characteristic decay time τ_μ and τ_u extracted from the fitting procedure of the $\Phi_\mu(t)$ and $\Phi_u(t)$ function respectively can thus be compared to the relaxation times determined from the BDS experiments for the I- and II-relaxation processes. Figure 7 shows that both times τ_μ and τ_u determined from the MD simulations roughly correspond to the

extrapolated lines in the high temperature range for the I- and II-relaxation processes. The agreement between BDS experiments and MD simulations is thus very reasonable. However, only one main process is seen from MD simulations while two processes, I and II, are observed from BDS. This discrepancy could origin from the progressive merging of the I- and II-relaxation processes upon increasing temperatures, which makes these processes indistinguishable in the MD simulations. Figure 9 also clearly reveals the presence of faster dynamical processes at very short time (10 to 100 ps) for both $\Phi_u(t)$ and $\Phi_\mu(t)$ functions. The characteristic times of these fast processes are clear outside of the BDS accessible time window and they were not analyzed in this work. They could be tentatively attributed to small and rapid rotational motions experienced by the TA molecules. In Figure 8.b, the time-evolution of the angle θ_u shows such small and rapid changes when the TA molecule is in one the preferable orientations (30° or 150°) which could explain the fast dynamical processes. Additional works are clearly required to identify their microscopic origin.

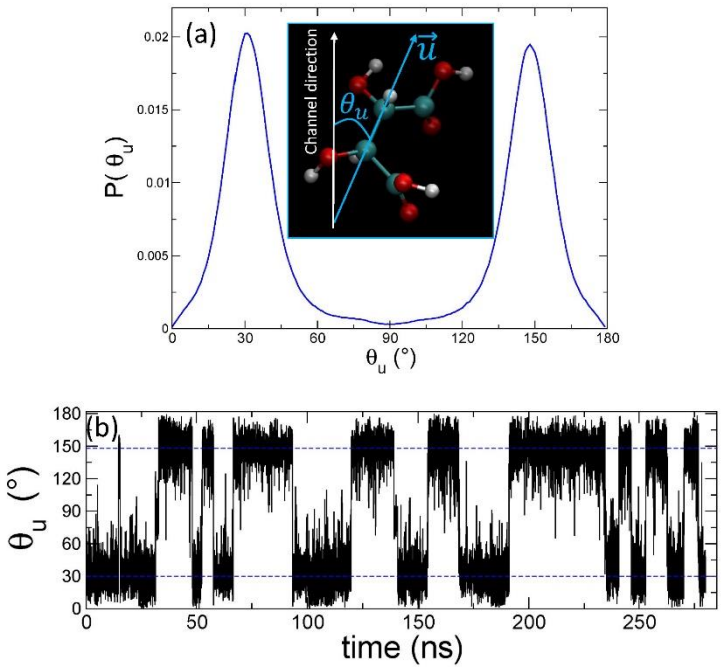

Figure 8. MD simulation results. (a) Distribution $P(\theta_u)$ of the orientation of the TA molecules in the channels at T = 550 K using the angle θ_u as a descriptor of the molecular orientation. In the inset, θ_u is defined as the angle between the vector $\vec{u}$ pointing along the central C-C bond of the

TA molecule and the direction of the channel. (b) Time-evolution of the angle θ_u for a targeted TA molecule.

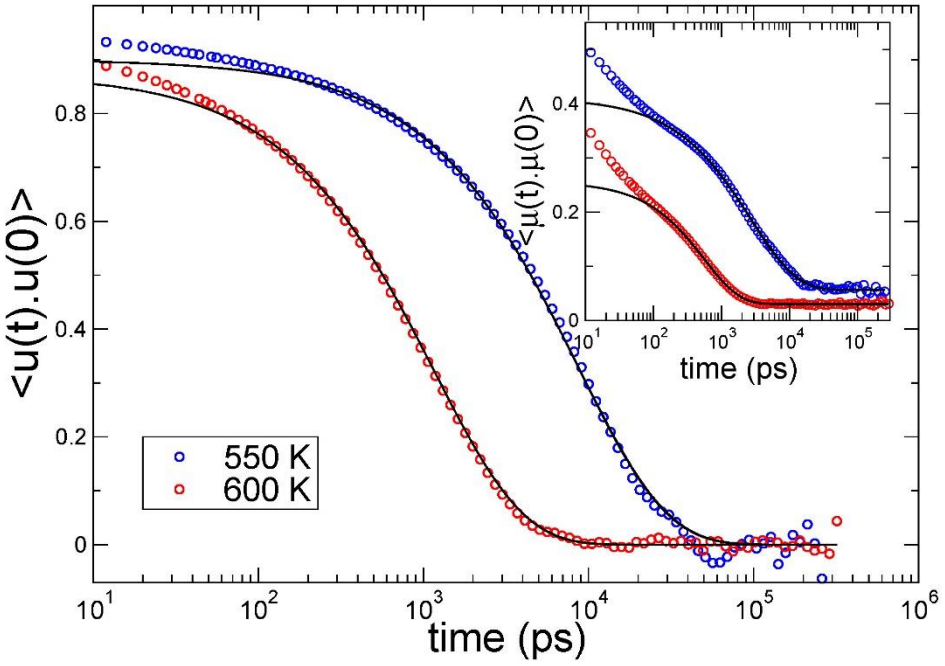

Figure 9. MD simulation results. Normalized time-dependent self-correlation function $\Phi_u(t) = \langle \vec{u}(t).\vec{u}(0) \rangle$ associated to the reorientation of the TA molecules in the cocrystal. The vector $\vec{u}$ is pointing along the central C-C bond of the TA molecule. In inset, normalized time-dependent self-correlation function $\Phi_u(t) = \langle \vec{\mu}(t).\vec{\mu}(0) \rangle$ associated to the reorientation of dipole moment of the TA molecules. Solid lines represent fits of the long-time decay using a stretched exponential function $f(t) = ae^{-(t/\tau)^{\beta}}$ where a, τ and β are the fitting parameters. β = 0.65 and 0.83 at 550 K and 600 K respectively.

Translational dynamics

The transport phenomena distinct from the classical Brownian motion found in confinement media having very narrow pores (about 1 nm) is particularly intriguing[12,14,34,15–18,22,23,29,32] but seems universal. It is tempting to use the present (disordered) CBZ:TA system to investigate the translation diffusion of the TA molecules in the narrow channels of about 1 nm size formed in the crystal. To the authors' knowledge, this is the first attempt to investigate this type of transport properties in this class of materials (cocrystal channel-like). In addition, the snapshots displayed in Figure 4 as well as the periodicity revealed in the axial density of the hydroxyl oxygen in Figure 5.a and the PDF of the centers of mass in Figure 5.b clearly suggest the

possible existence of some files of TA molecules in the channels and then a possible single-file motion. Figure 10.a shows the trajectory as function of time along the channel direction of some targeted neighboring TA molecules belonging to the same channel. Other trajectories of some targeted neighboring TA molecules are also provided as supplementary materials (Figure S7). Figure 10.a demonstrates the presence of translational dynamics of the TA molecules in addition to the rotation dynamics shown in the previous section. The low number of HBs formed between TA molecules as described before and the presence of "empty spaces" in the channels (see Figure 4.b) should certainly facilitate this translational mobility. The trajectory can be roughly described as small fluctuations of about 1 Å combined larger hops of about 6 Å to 7 Å. The extend of these hops is consistent with the distance between the centers of mass shown in Figure 5.b. The trajectory of the molecules seems also very correlated well in line with a possible single-file diffusion process. It should be also noted that in all analyzed trajectories, we do not observe TA molecules passing each other due the small size of the channel. However, a more detailed analysis of the trajectories for all molecules belonging to the same channels reveals some decorrelations at long times between the motions of neighboring molecules and between non-neighboring molecules (Figure S7). Indeed, the channels of the cocrystal CBZ:TA are not completely filled (see Figure 4.c). Thus, there are some empty spaces between some groups of TA molecules. They actually enable the molecules to not move in the same direction as it should be expected in a perfect single-file diffusion process. In the optimized structure (T = 0 K), calculations performed from MD simulations show that channels are filled by 25% of single chains, *i.e.* one non-interrupted chain of TA molecules, and 75% of two chains, *i.e.* two chains of TA molecules separated by one empty space. At T = 550 K, we found 40%, 50% and 10% of single chains, two chains and three chains respectively. At T = 600 K, the distribution becomes 16%, 52%, 28% and 4% of single chains, two chains, three chains and four chains respectively. These statistics nicely

demonstrate the increased number of chains in the organization of the channels upon increasing temperature and thus the possibility for the translation dynamics to not evolve following the single-file dynamics. In Figure 10.b, this trend is confirmed based on the calculation of the mean square displacement (MSD) $\langle r^2(t)\rangle$. MSDs have been calculated for all TA molecules along the three crystallographic axes $\vec{a}$, $\vec{b}$ and $\vec{c}$. $(\vec{a}, \vec{b})$ is in the plane of the channel while $\vec{c}$ is along the direction of the channel (see Figure 4.a and Figure 4.c). As expected, diffusion along $\vec{a}$ and $\vec{b}$ is actually very limited as demonstrated by the very small value of the MSD computed between 0.1 and 1 Å^2. TA molecules cannot obviously cross the space occupied by the CBZ molecules and cannot move from one channel to the neighboring channel. Oppositely, a clear diffusion is observed along the direction of channel $\vec{c}$. The MSD along $\vec{c}$ cannot not be adjusted using just a single diffusion law. Figure 10.b shows that two diffusion laws are clearly necessary to reproduce the global behavior of the MSD $\langle r^2(t)\rangle$ as function of time. At short time, the MSD can be fitted by the law $\langle r^2(t)\rangle \sim t^{1/2}$ which is classically associated to the single-file diffusion process.[12,14,34,15–18,22,23,29,32] At longer times, Figure 10.b also shows a change and the classical diffusion law $\langle r^2(t)\rangle \sim t$ corresponding to Fickian motion is recovered. Interestingly, this transition between two diffusion mechanisms is therefore seen in the present disordered cocrystal as reported in other systems.[16,18,29] The crossing between both types of diffusion is found in the range $\langle r^2(t)\rangle \approx$ 25 Å^2 to 36 Å^2, thus, roughly corresponding to a displacement of the molecules of about 5 Å to 6 Å. This distance is close to the small hop distance of ca. 6 to 7 Å, well in line with the distance between the centers of mass shown in Figure 5.b. Tentatively, one may suggest that molecules first start moving as "single-file" but just over about one hop distance. In this regime, the molecules are confined to advancing one behind the other in the same direction since the narrow channels size (1 nm) exclude mutual passages of the molecules along the channel. Then, at longer times, they are allowed to move following the classical Brownian process. It is important to note that the single-file diffusion

$\langle r^2(t)\rangle \sim t^{1/2}$ is actually fully correct for hypothetical infinitely long channels.[29] Periodic boundary conditions are used in the present MD simulations so channels could be considered as infinite. However, the TA molecules in the channels are not organized as one long single file but as several shorter files made of few molecules separated by empty spaces (see Figure 4.b) as analyzed previously. It seems reasonable that the single-file diffusion mechanism may not persist at longer times since molecules have the possibility to use these empty spaces for their moves in a not correlated way. Further investigations should be performed in order to confirm these preliminary findings. The size of the required systems (see materials & methods) and CPU computations times do not presently enable the authors to fully analyses translational dynamics in more details.

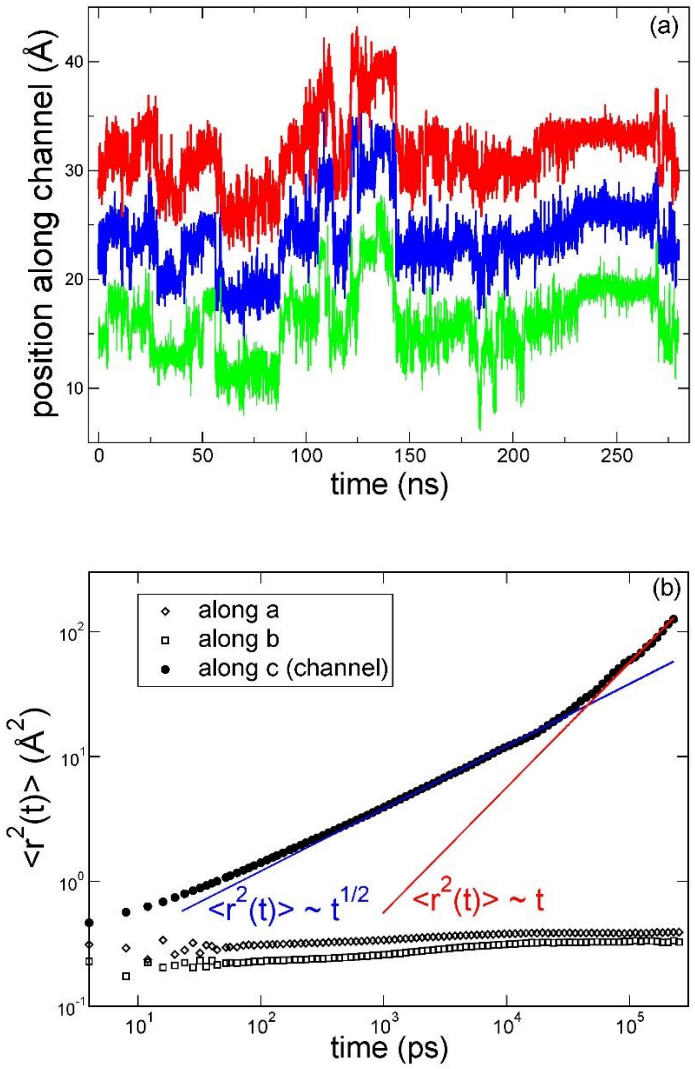

Figure 10. MD simulation results obtained T = 550 K. (a) Position of the center of mass as function of time along the channel direction of three neighboring TA molecules belonging to the same channel. (b) Mean square displacement $\langle r^2(t)\rangle$ of the TA molecules (center of mass) along the three crystallographic directions ($\vec{a}$, $\vec{b}$ and $\vec{c}$). The channels are orientated along the c direction (see also Figure 3). Solid lines indicate fits using two diffusion laws: $\langle r^2(t)\rangle \sim t^{1/2}$ describing a single-file diffusion process and $\langle r^2(t)\rangle \sim t$ corresponding to the normal diffusion (Fickian).

CONCLUSIONS

In this article, we have analyzed the nature of the structural and dynamical disorder in the organic cocrystal CBZ:TA exhibiting a true nanometric channel-like architecture in which disordered TA molecules are filling the CBZ based channels. By means of complementary solid-state NMR, X-ray diffraction and dielectric relaxation spectroscopy experiments combined with molecular dynamics simulations, the structural organization and intermolecular HB interactions, rotational and translational dynamics have been in deep discussed.

We find that the TA molecules in the channels are partially disordered as shown by solid-state NMR. Oppositely, a clear partial organized structure is detected based on the radial density of the hydroxyl groups and PDF of the centers of mass computed along the channel by MD simulations. The organization of the molecules in the channel can be simply described as one-dimension files of molecules whose centers of mass are separated by *ca*. 6 to 7 Å. TA molecules are weakly hydrogen-bonded between them but strongly hydrogen-bonded with the CBZ molecules forming the channels. TA molecules do not form a single long file in the channels but several files composed of molecules separated by some empty spaces. A large number of very well formed HBs is found between the –OH hydroxyl groups of the TA molecules and the C=O group of the carboxamide CBZ molecules. It can be thus concluded that the TA molecules organization is completely driven by the ordered CBZ channels through intermolecular HBs. These latter are actually not static. HBs can break and reform and it enables molecular mobility.

It is demonstrated experimentally that TA molecules in the channels show rotational dynamics using dielectric relaxation spectroscopy which is a technique of choice to investigate molecular mobility. A thorough analysis reveals the presence of two relaxation processes characterized by an Arrhenius temperature dependence, with activation energies of about 58 and 67 kJ·mol^{-}

[1] well in line with the values reported for local processes in HB liquids. Interestingly, there is evidence of the suppression (freezing out) of the molecular mobility in the temperature range [173, 193] K concomitantly with the presence of a kink in the temperature evolution of the crystalline cell volume which is usually associated with the glass transition phenomenon. It reveals a remarkable link between the molecular mobility of the TA molecules and the CBZ:TA crystal anharmonicity. Rotational dynamics is confirmed by MD simulations which also show that TA molecules adopt preferable orientations with the direction of the channel. Molecular motions could thus be interpreted as rotational jumps between preferred orientations.

It is demonstrated that TA molecules in the channels show translational dynamics by MD simulations. Molecular motion occurs by small hops of *ca*. 6 to 7 Å consistent with the distance between first neighbors determined by the PDF analysis. At short times, the single-file diffusion process is revealed while at longer times the classical diffusion (Fickian) is recovered. This transition between the two diffusion mechanisms is explained by the presence of the empty spaces in the channels which creates several short files instead of a single long file and which thus offers to the molecules the possibility to have uncorrelated motions.

This work is a first attempt to demonstrate that disordered channel-like cocrystals offer a new type of interesting nanoconfinement environments. It clearly motivates to test the universality of our findings on other cocrystalline systems. Several examples of molecules with different sizes, shapes or HB properties able to form disordered channel-like structure with carbamazepine have been proposed by Childs *et al.*[47] The single-file diffusion and its transition to the classical diffusion mechanism suggested by MD simulations clearly challenge experimentalists for a validation. To our knowledge, this is the first study to fully understand the exact nature of the disorder (partial, total, translational, orientational, static or dynamic) for

this class of materials. Such understanding presents a fundamental significance, but also a possible interest for the control of particle transport in chemical and pharmaceutical processes.

MATERIALS AND METHODS

Experiments.

Materials. Carbamazepine (form III) from Duchefa Farma BV (purity 99.8%) and L-tartaric acid from Sigma-Aldrich (purity ≥99.5%) were used as supplied, without further purification.

Cocrystal Synthesis.

CBZ:TA cocrystal was prepared by liquid-assisted grinding stoichiometric amounts of crystalline parent components, CBZ (form III) and L-TA, at a (3:1) molar ratio. Grinding was performed at room temperature using a Mixer Mill MM 400 from Retsch, at 30 Hz for a total time of 30 min. A small volume of acetonitrile (10 μL for each 100 mg of mixture) was added to the physical mixture of crystalline parent components before grinding.[84] The thermal stability of the synthetized CBZ:TA cocrystalline phase in the explored temperature range was first confirmed by differential scanning calorimetry (Figure S3). The cocrystal is thermally stable up to the onset of melting ($T_{m,onset}$ = 418 K). No loss of TA molecules is detected till melting. No solid-solid transition has occurred from 123 K to 373 K, as confirmed by PXRD measurements at variable temperature (Figure S4.a).

Powder X-Ray Diffraction (PXRD). Powder X-Ray diffraction analysis was carried with a PANalytical X'Pert pro MPD diffractometer equipped with a Cu X-ray tube (selected wavelength λCuKα = 1.54056 Å) and a X'celerator detector. The powder samples were enclosed in a 0.7 mm diameter Lindemann glass capillary, which was rotating around their vertical axis during data collection to reduce the effect of a possible preferential orientation. The diffraction patterns were collected by steps of 0.0167° (in 2-theta) over the angular range 3–60°, with a counting time of 50s per step.

Solid State NMR. $^{1}H–^{13}C$ cross-polarization magic angle spinning (CP/MAS) solid-state NMR spectra were acquired on a Bruker Avance III solid-state NMR spectrometer equipped with a triple resonance probe operating at 400.23 MHz for ^{1}H and 100.64 MHz for ^{13}C equipped with magic angle spinning. The powder of each sample was packed in 4 mm zirconia rotors with Kel-F caps. These were rotated at an MAS rate of 10 KHz. The spectra were acquired at 298 K. The Hartmann–Hahn conditions for $^{1}H–^{13}C$ CP/MAS experiments were set using hexamethylbenzene (HMB) and all spectra were referenced to external tetramethylsilane (TMS). $^{1}H–^{13}C$ CP/MAS NMR spectra were acquired using $_{1}H$ $\pi/2$ pulse length of 4.5 μs and $^{1}H–^{13}C$ CP contact time of 2000 μs. For the CBZ:TA cocrystal and TA, 128 scans were acquired with a pulse delay optimized to 20 s and for CBZ form III had 32 scans acquired with a pulse delay of 100 seconds.

Broadband Dielectric Spectroscopy. Dielectric measurements were carried out using a Novocontrol Technologies GmbH Alpha Analyzer in the frequency range from 10^{-2} to 10^{7} Hz at temperatures ranging from 143 to 373 K (in isothermal steps of 2 degrees). The powder of each sample was slightly compressed between two gold-plated electrodes (diameter of 1 cm). The temperature regulation was managed by a Quatro cryo-system (Novocontrol) with a temperature stability better than 0.2 K, using a gas stream being evaporated from a liquid nitrogen Dewar.

The dielectric spectra (imaginary and real part) were analyzed by fitting a sum of the phenomenological Cole-Cole (CC) function[64,71] to the isothermal data:

$$\varepsilon^*(\omega) = \varepsilon'(\omega) - i\varepsilon''(\omega) = \varepsilon_\infty + \frac{\Delta\varepsilon}{1+(i\omega\tau_{CC})^{\beta CC}} \quad (1)$$

where ω is the angular frequency; $\Delta\varepsilon = \varepsilon_s - \varepsilon_\infty$ is the dielectric strength; ε_s and ε_∞ are the low-frequency and high-frequency limits of $\varepsilon'(\omega)$, respectively. τ_{CC} is a characteristic relaxation time at which $\varepsilon''(\omega)$ is maximum ($\tau_{CC} = \tau = 1/(2\pi\nu_{max})$), and the exponent β_{CC}

($0 < \beta_{CC} < 1$) referred to as a measure of a symmetric broadening of the $\varepsilon''(\omega)$ peak compared to the Debye function ($\beta_{CC} = 1$) valid for non-interacting dipoles. Deviations from the Debye behavior usually indicate a distribution of relaxation times, typical of disordered systems. The smaller the β_{CC} values, the wider the distribution of relaxation times. Solid lines in Figure 6.a and Figure S2 are a sum of two CC functions describing the I- and II-relaxation processes.

Simulations

Molecular dynamics (MD) simulations have been performed using the DL_POLY package[85] and the GAFF force field[86] (General Amber Force Field). This force field was chosen due to its capability of reproducing successfully large number of experimental data of low molecular weight molecules.[87] As recommended for the GAFF force field,[86] atomic partial charges were calculated from ab-initio computations using the Gaussian program at the HF/6-31G* level[63] with the restrained electrostatic potential (RESP) fitting approach. Electrostatic contribution was computed by using the Ewald sum with a convergence parameter of 0.36 $Å^{-1}$. For both van der Waals and electrostatic interactions, the same cutoff radius of 10 Å was employed. Periodic boundary conditions were applied in all directions. The time step to integrate Newton's equation of motion was chosen to 0.001 ps. Simulations have been conducted either in the NPT or NVT statistical ensemble where P is the pressure, T the temperature and V the volume. Pressure and temperature were controlled with a Nose-Hoover barostat and thermostat respectively. All NPT simulations were realized at atmospheric pressure. The Nosé Hoover thermostat and barostat relaxation times have been set at 0.2 and 2.0 ps respectively. The equilibrated volume of the simulation box during the NPT simulation was considered to compute the averaged density of system and used to perform the subsequent production simulation in the NVT ensemble. MD simulations were performed at three temperatures 530 K, 550 K and 600 K. Since periodic boundary conditions are used in the MD simulations, it is

possible to overheat the crystalline state even at very high temperatures above the melting temperature ($T_{m,peak}$ = 431 K; see Figure S3) without melting the structure. We have systematically checked that the overall channel-like structure formed by the CBZ molecules is thus always maintained.

The equilibration/production times range from 10/120 ns to 20/250 ns from the highest to the lowest investigated temperature. Two systems have been investigated. A crystal (31Å x 28 Å x 31 Å) composed of a total of 72 CBZ molecules and 24 TA molecules. This crystal possesses 6 "short" channels including 4 TA molecules each. A crystal (21 Å x 28 Å x 126 Å) composed of a total of 192 CBZ molecules and 64 TA molecules. It possesses 4 "long" channels including 16 TA molecules each. The L enantiomer is used for the TA molecules. In order to generate the initial atomic positions of the CBZ molecules in the crystalline structure, we have used the MOXWIG[47] structure (a = 10.300 6 Å, b=26.972 Å , c = 5.0718 Å, β = 104.235°, Z = 4 , $P2_1/c$) available at the Cambridge Structural Database.[46] Then, the relevant number of TA molecules was inserted in the channels with random positions in order to maintain the required stoichiometry (3:1). It should be noted that a few MD simulations have been performed in which the position of the CBZ atoms are fixed in order to generate PXRD patterns using the VESTA program[88] for a comparison with the PXRD obtained from experiments or generate based on the published MOXWIG[47] structure. By fixing CBZ atoms, Bragg peaks positions originating from CBZ atoms are thus maintained at the same positions in the PXRD patterns and it thus allows discussing the impact of the TA molecules on the PXRD pattern more easily. The density of the model of the CBZ:TA cocrystal computed by MD simulations is about 1.38 g/cm^3 at T = 0 K and 1.26 at T = 550 K. The experimental density is about 1.40 g/cm^3 at 173 K and 1.39 g/cm^3 at 298 K. A precise comparison cannot be performed with the experimental data since different temperatures have been investigated. However, the agreement seems reasonable for a classical force-field.

ASSOCIATED CONTENT

Supporting Information

Figures of dielectric spectra, calorimetric and PXRD data.
Figures of MD simulations (PDF).

ACKNOWLEDGMENTS

This project has received funding from the Interreg 2 Seas program 2014-2020 co-funded by the European Regional Development Fund under subsidy contracts 2S01-059_IMODE and 2S07-033_ Site Drug.

The project ARCHI-CM, Chevreul Institute (FR 2638), Ministère de l'Enseignement Supérieur et de la Recherche, Région Hauts-de-France and European Regional Development Fund (FEDER) are also acknowledged for supporting and funding this work.

We are grateful to NMR platform of UEA Faculty of Science Analytical Facilities for NMR experiments.

ABBREVIATIONS

CBZ, carbamazepine; TA, tartaric acid; LAG, liquid assisted grinding; BDS, broadband dielectric spectroscopy; MD, Molecular Dynamics; MSD, mean square displacement

REFERENCES

(1) Domanov, Y. A.; Aimon, S.; Toombes, G. E. S.; Renner, M.; Quemeneur, F.; Triller, A.; Turner, M. S.; Bassereau, P. Mobility in Geometrically Confined Membranes. *Proc. Natl. Acad. Sci. U. S. A.* **2011**, *108* (31), 12605–12610. https://doi.org/10.1073/pnas.1102646108.

(2) Gorshunov, B. P.; Zhukova, E. S.; Torgashev, V. I.; Lebedev, V. V.; Shakurov, G. S.; Kremer, R. K.; Pestrjakov, E. V.; Thomas, V. G.; Fursenko, D. A.; Dressel, M. Quantum Behavior of Water Molecules Confined to Nanocavities in Gemstones. *J. Phys. Chem. Lett.* **2013**, *4* (12), 2015–2020. https://doi.org/10.1021/jz400782j.

(3) Aoun, B.; Russo, D. Nano-Confinement of Biomolecules: Hydrophilic Confinement Promotes Structural Order and Enhances Mobility of Water Molecules. *Nano Res.* **2016**, *9* (2), 273–281. https://doi.org/10.1007/s12274-015-0907-7.

(4) Ghandi, K.; Landry, C.; Du, T.; Lainé, M.; Saul, A.; Le Caër, S. Influence of Confinement on Free Radical Chemistry in Layered Nanostructures. *Sci. Rep.* **2019**, *9* (1), 1–13. https://doi.org/10.1038/s41598-019-52662-z.

(5) Busselez, R.; Lefort, R.; Ji, Q.; Affouard, F.; Morineau, D. Molecular Dynamics Simulation of Nanoconfined Glycerol. *Phys. Chem. Chem. Phys.* **2009**, *11* (47), 11127–11133. https://doi.org/10.1039/b911859d.

(6) Brás, A. R.; Merino, E. G.; Neves, P. D.; Fonseca, I. M.; Dionísio, M.; Schönhals, A.; Correia, N. T. Amorphous Ibuprofen Confined in Nanostructured Silica Materials: A Dynamical Approach. *J. Phys. Chem. C* **2011**, *115* (11), 4616–4623. https://doi.org/10.1021/jp107631m.

(7) Adrjanowicz, K.; Kolodziejczyk, K.; Kipnusu, W. K.; Tarnacka, M.; Mapesa, E. U.; Kaminska, E.; Pawlus, S.; Kaminski, K.; Paluch, M. Decoupling between the Interfacial and Core Molecular Dynamics of Salol in 2D Confinement. *J. Phys. Chem. C* **2015**, *119* (25), 14366–14374. https://doi.org/10.1021/acs.jpcc.5b01391.

(8) Nartowski, K. P.; Malhotra, D.; Hawarden, L. E.; Fábián, L.; Khimyak, Y. Z. Nanocrystallization of Rare Tolbutamide Form V in Mesoporous MCM-41 Silica. *Mol. Pharm.* **2018**, *15* (11), 4926–4932. https://doi.org/10.1021/acs.molpharmaceut.8b00575.

(9) Mhanna, R.; Catrou, P.; Dutta, S.; Lefort, R.; Essafri, I.; Ghoufi, A.; Muthmann, M.; Zamponi, M.; Frick, B.; Morineau, D. Dynamic Heterogeneities in Liquid Mixtures Confined in Nanopores. *J. Phys. Chem. B* **2020**, *124* (15), 3152–3162. https://doi.org/10.1021/acs.jpcb.0c01035.

(10) Sarfati, R.; Schwartz, D. K. Temporally Anticorrelated Subdiffusion in Water Nanofilms on Silica Suggests Near-Surface Viscoelasticity. *ACS Nano* **2020**, *14* (3), 3041–3047. https://doi.org/10.1021/acsnano.9b07910.

(11) Mamontov, E.; Kumzerov, Y. A.; Vakhrushev, S. B. Diffusion of Benzene Confined in the Oriented Nanochannels of Chrysotile Asbestos Fibers. *Phys. Rev. E - Stat. Nonlinear, Soft Matter Phys.* **2005**, *72* (5), 1–7. https://doi.org/10.1103/PhysRevE.72.051502.

(12) Anovitz, L. M.; Mamontov, E.; Ben Ishai, P.; Kolesnikov, A. I. Anisotropic Dynamics of Water Ultraconfined in Macroscopically Oriented Channels of Single-Crystal Beryl: A Multifrequency Analysis. *Phys. Rev. E - Stat. Nonlinear, Soft Matter Phys.* **2013**, *88* (5), 1–16. https://doi.org/10.1103/PhysRevE.88.052306.

(13) Yaghi, O. M.; Li, H. Hydrothermal Synthesis of a Metal-Organic Framework Containing Large Rectangular Channels. *J. Am. Chem. Soc.* **1995**, *117* (41), 10401–10402. https://doi.org/10.1021/ja00146a033.

(14) Ghoufi, A.; Maurin, G. Single-File Diffusion of Neo-Pentane Confined in the MIL-47(V) Metal-Organic Framework. *J. Phys. Chem. C* **2019**, *123* (28), 17360–17367. https://doi.org/10.1021/acs.jpcc.9b04308.

(15) Hahn, K.; Kärger, J. Deviations from the Normal Time Regime of Single-File Diffusion. *J. Phys. Chem. B* **1998**, *102* (30), 5766–5771. https://doi.org/10.1021/jp981039h.

(16) Nelson, P. H.; Auerbach, S. M. Self-Diffusion in Single-File Zeolite Membranes Is Fickian at Long Times. *J. Chem. Phys.* **1999**, *110* (18), 9235–9243. https://doi.org/10.1063/1.478847.

(17) Schüring, A.; Vasenkov, S.; Fritzsche, S. Influence of Boundaries of Nanoporous Crystals on Molecular Exchange under the Conditions of Single-File Diffusion. *J. Phys. Chem. B* **2005**, *109* (35), 16711–16717. https://doi.org/10.1021/jp052314k.

(18) Yang, X.; Wu, M.; Qin, Z.; Wang, J.; Wen, T. Molecular Dynamics Simulations on Single-File Diffusions: Effects of Channel Potential Periods and Particle-Particle Interactions. *J. Appl. Phys.* **2009**, *106* (8), 084905. https://doi.org/10.1063/1.3247576.

(19) Sastre, G.; Corma, A. The Confinement Effect in Zeolites. *J. Mol. Catal. A Chem.* **2009**, *305* (1–2), 3–7. https://doi.org/10.1016/j.molcata.2008.10.042.

(20) Ngai, K. L.; Lunkenheimer, P.; Loidl, A. Predicting the α-Relaxation Time of Glycerol Confined in 1.16 Nm Pores of Zeolitic Imidazolate Frameworks. *Phys. Chem. Chem. Phys.* **2020**, *22* (2), 507–511. https://doi.org/10.1039/C9CP05270D.

(21) Huwe, A.; Kremer, F.; Behrens, P.; Schwieger, W. Molecular Dynamics in Confining Space: From the Single Molecule to the Liquid State. *Phys. Rev. Lett.* **1999**, *82* (11), 2338–2341. https://doi.org/10.1103/PhysRevLett.82.2338.

(22) Striolo, A. The Mechanism of Water Diffusion in Narrow Carbon Nanotubes. *Nano Lett.* **2006**, *6* (4), 633–639. https://doi.org/10.1021/nl052254u.

(23) Das, A.; Jayanthi, S.; Deepak, H. S. M. V.; Ramanathan, K. V.; Kumar, A.; Dasgupta, C.; Sood, A. K. Single-File Diffusion of Confined Water inside SWNTs: An NMR Study. *ACS Nano* **2010**, *4* (3), 1687–1695. https://doi.org/10.1021/nn901554h.

(24) Pan, X.; Bao, X. The Effects of Confinement inside Carbon Nanotubes on Catalysis. *Acc. Chem. Res.* **2011**, *44* (8), 553–562. https://doi.org/10.1021/ar100160t.

(25) Toudic, B.; Le Lann, H.; Guillaume, F.; Lechner, R. E.; Ollivier, J.; Bourges, P. Coherent Neutron Scattering Analysis of Alkane Dynamical Disorder inside Nanoporous Urea Intergrowth Crystals. *Chem. Phys.* **2003**, *292* (2–3), 191–199. https://doi.org/10.1016/S0301-0104(03)00249-0.

(26) Guo, Y.; Guo, S.; Ren, J.; Zhai, Y.; Dong, S.; Wang, E. Cyclodextrin Functionalized Graphene Nanosheets with High Supramolecular Recognition Capability: Synthesis and Host−Guest Inclusion for Enhanced Electrochemical Performance. *ACS Nano* **2010**, *4* (7), 4001–4010. https://doi.org/10.1021/nn100939n.

(27) Liu, C.; Zhao, H.; Hou, P.; Qian, B.; Wang, X.; Guo, C.; Wang, L. Efficient Graphene/Cyclodextrin-Based Nanocontainer: Synthesis and Host–Guest Inclusion for Self-Healing Anticorrosion Application. *ACS Appl. Mater. Interfaces* **2018**, *10* (42), 36229–36239. https://doi.org/10.1021/acsami.8b11108.

(28) Sandilya, A. A.; Natarajan, U.; Priya, M. H. Molecular View into the Cyclodextrin Cavity: Structure and Hydration. *ACS Omega* **2020**, *5* (40), 25655–25667. https://doi.org/10.1021/acsomega.0c02760.

(29) Bowers, C. R.; Dvoyashkin, M.; Salpage, S. R.; Akel, C.; Bhase, H.; Geer, M. F.; Shimizu, L. S. Crystalline Bis-Urea Nanochannel Architectures Tailored for Single-File Diffusion Studies.

ACS Nano **2015**, *9* (6), 6343–6353. https://doi.org/10.1021/acsnano.5b01895.

(30) Li, R.; Fan, J.; Li, H.; Yan, X.; Yu, Y. Dynamic Behaviors and Transport Properties of Ethanol Molecules in Transmembrane Cyclic Peptide Nanotubes. *J. Chem. Phys.* **2015**, *143* (1). https://doi.org/10.1063/1.4923010.

(31) Calvelo, M.; Lynch, C. I.; Granja, J. R.; Sansom, M. S. P.; Garcia-Fandiño, R. Effect of Water Models on Transmembrane Self-Assembled Cyclic Peptide Nanotubes. *ACS Nano* **2021**, *15* (4), 7053–7064. https://doi.org/10.1021/acsnano.1c00155.

(32) Yang, S. Y.; Yang, J. A.; Kim, E. S.; Jeon, G.; Oh, E. J.; Choi, K. Y.; Hahn, S. K.; Kim, J. K. Single-File Diffusion of Protein Drugs through Cylindrical Nanochannels. *ACS Nano* **2010**, *4* (7), 3817–3822. https://doi.org/10.1021/nn100464u.

(33) Musteata, V. E.; Chisca, S.; Meneau, F.; Smilgies, D. M.; Nunes, S. P. Carboxyl-Functionalized Nanochannels Based on Block Copolymer Hierarchical Structures. *Faraday Discuss.* **2018**, *209*, 303–314. https://doi.org/10.1039/c8fd00015h.

(34) Horner, A.; Pohl, P. Single-File Transport of Water through Membrane Channels. *Faraday Discuss.* **2018**, *209*, 9–33. https://doi.org/10.1039/c8fd00122g.

(35) Martelli, F.; Crain, J.; Franzese, G. Network Topology in Water Nanoconfined between Phospholipid Membranes. *ACS Nano* **2020**, *14* (7), 8616–8623. https://doi.org/10.1021/acsnano.0c02984.

(36) Leoni, F.; Calero, C.; Franzese, G. Nanoconfined Fluids: Uniqueness of Water Compared to Other Liquids. *ACS Nano* **2021**, *15* (12), 19864–19876. https://doi.org/10.1021/acsnano.1c07381.

(37) Aakeröy, C. B.; Salmon, D. J. Building Co-Crystals with Molecular Sense and Supramolecular Sensibility. *CrystEngComm* **2005**, *7* (72), 439–448. https://doi.org/10.1039/b505883j.

(38) Schultheiss, N.; Newman, A. Pharmaceutical Cocrystals and Their Physicochemical Properties. *Cryst. Growth Des.* **2009**, *9* (6), 2950–2967. https://doi.org/10.1021/cg900129f.

(39) Springuel, G.; Norberg, B.; Robeyns, K.; Wouters, J.; Leyssens, T. Advances in Pharmaceutical Co-Crystal Screening: Effective Co-Crystal Screening through Structural Resemblance. *Cryst. Growth Des.* **2012**, *12* (1), 475–484. https://doi.org/10.1021/cg201291k.

(40) Leyssens, T.; Horst, J. H. ter. 9. Solution Co-Crystallisation and Its Applications. In *Multi-Component Crystals*; Tiekink, E., Zukerman, J., Eds.; De Gruyter: Berlin, Boston, 2017; pp 205–236. https://doi.org/10.1515/9783110464955-009.

(41) Karimi-Jafari, M.; Padrela, L.; Walker, G. M.; Croker, D. M. Creating Cocrystals: A Review of Pharmaceutical Cocrystal Preparation Routes and Applications. *Cryst. Growth Des.* **2018**, *18* (10), 6370–6387. https://doi.org/10.1021/acs.cgd.8b00933.

(42) Rupasinghe, T. P.; Hutchins, K. M.; Bandaranayake, B. S.; Ghorai, S.; Karunatilake, C.; Bučar, D.-K.; Swenson, D. C.; Arnold, M. A.; MacGillivray, L. R.; Tivanski, A. V. Mechanical Properties of a Series of Macro- and Nanodimensional Organic Cocrystals Correlate with Atomic Polarizability. *J. Am. Chem. Soc.* **2015**, *137* (40), 12768–12771. https://doi.org/10.1021/jacs.5b07873.

(43) Corpinot, M. K.; Bučar, D.-K. A Practical Guide to the Design of Molecular Crystals. *Cryst. Growth Des.* **2019**, *19* (2), 1426–1453. https://doi.org/10.1021/acs.cgd.8b00972.

(44) Dudek, M. K.; Wielgus, E.; Paluch, P.; Śniechowska, J.; Kostrzewa, M.; Day, G. M.; Bujacz, G. D.; Potrzebowski, M. J. Understanding the Formation of Apremilast Cocrystals. *Acta Crystallogr. Sect. B Struct. Sci. Cryst. Eng. Mater.* **2019**, *75*, 803–814. https://doi.org/10.1107/S205252061900917X.

(45) Wright, S. E.; Cole, J. C.; Cruz-Cabeza, A. J. Conformational Change in Molecular Crystals: Impact of Solvate Formation and Importance of Conformational Free Energies. *Cryst. Growth Des.* **2021**, *21* (12), 6924–6936. https://doi.org/10.1021/acs.cgd.1c00833.

(46) Groom, C. R.; Bruno, I. J.; Lightfoot, M. P.; Ward, S. C. The Cambridge Structural Database. *Acta Crystallogr. Sect. B Struct. Sci. Cryst. Eng. Mater.* **2016**, *72* (2), 171–179. https://doi.org/10.1107/S2052520616003954.

(47) Childs, S. L.; Wood, P. A.; Rodríguez-Hornedo, N.; Reddy, L. S.; Hardcastle, K. I. Analysis of 50 Crystal Structures Containing Carbamazepine Using the Materials Module of Mercury CSD. *Cryst. Growth Des.* **2009**, *9* (4), 1869–1888. https://doi.org/10.1021/cg801056c.

(48) Schneider-Rauber, G.; Arhangelskis, M.; Bond, A. D.; Ho, R.; Nere, N.; Bordawekar, S.; Sheikh, A. Y.; Jones, W. Polymorphism and Surface Diversity Arising from Stress-Induced Transformations-the Case of Multicomponent Forms of Carbamazepine. *Acta Crystallogr. Sect. B Struct. Sci. Cryst. Eng. Mater.* **2021**, *77*, 54–67. https://doi.org/10.1107/S2052520620015437.

(49) Cruz Cabeza, A. J.; Day, G. M.; Motherwell, W. D. S.; Jones, W. Solvent Inclusion in Form II Carbamazepine. *Chem. Commun.* **2007**, *12* (16), 1600–1602. https://doi.org/10.1039/b701299c.

(50) Rossi, B.; Verrocchio, P.; Viliani, G.; Mancini, I.; Guella, G.; Rigo, E.; Scarduelli, G.; Mariotto, G. Vibrational Properties of Ibuprofen-Cyclodextrin Inclusion Complexes Investigated by Raman Scattering and Numerical Simulation. *J. Raman Spectrosc.* **2009**, *40* (4), 453–458. https://doi.org/10.1002/jrs.2150.

(51) Fabbiani, F. P. A.; Byrne, L. T.; McKinnon, J. J.; Spackman, M. A. Solvent Inclusion in the Structural Voids of Form II Carbamazepine: Single-Crystal X-Ray Diffraction, NMR Spectroscopy and Hirshfeld Surface Analysis. *CrystEngComm* **2007**, *9* (9), 728. https://doi.org/10.1039/b708303n.

(52) Prohens, R.; Font-Bardia, M.; Barbas, R. Water Wires in the Nanoporous Form II of Carbamazepine: A Single-Crystal X-Ray Diffraction Analysis. *CrystEngComm* **2013**, *15* (5), 845–847. https://doi.org/10.1039/c2ce26787j.

(53) Childs, S. L.; Rodríguez-Hornedo, N.; Reddy, L. S.; Jayasankar, A.; Maheshwari, C.; McCausland, L.; Shipplett, R.; Stahly, B. C. Screening Strategies Based on Solubility and Solution Composition Generate Pharmaceutically Acceptable Cocrystals of Carbamazepine. *CrystEngComm* **2008**, *10* (7), 856. https://doi.org/10.1039/b715396a.

(54) Hill, H. D. W.; Zens, A. P.; John, J. Solid-State NMR Spectroscopy. Distinction of Diastereomers and Determination of Optical Purity. *J. Am. Chem. Soc.* **1979**, *101* (23), 7090–7091. https://doi.org/10.1021/ja00517a063.

(55) Fukami, T.; Tahara, S.; Yasuda, C.; Nakasone, K. Structural Refinements and Thermal Properties of L(+)-Tartaric, D(–)-Tartaric, and Monohydrate Racemic Tartaric Acid. *Int. J. Chem.* **2016**, *8* (2), 9–21. https://doi.org/10.5539/ijc.v8n2p9.

(56) Harris, R. K.; Ghi, P. Y.; Puschmann, H.; Apperley, D. C.; Griesser, U. J.; Hammond, R. B.; Ma, C.; Roberts, K. J.; Pearce, G. J.; Yates, J. R.; Pickard, C. J. Structural Studies of the Polymorphs of Carbamazepine, Its Dihydrate, and Two Solvates. *Org. Process Res. Dev.* **2005**, *9* (6), 902–910. https://doi.org/10.1021/op0500990.

(57) Reboul, J. P.; Cristau, B.; Soyfer, J. C.; Astier, J. P. 5H-Dibenz[b,f]Azépinecarboxamide-5 (Carbamazépine). *Acta Crystallogr. Sect. B Struct. Crystallogr. Cryst. Chem.* **1981**, *37* (10), 1844–1848. https://doi.org/10.1107/S0567740881007383.

(58) Albertsson, J.; Oskarsson, Å.; Ståhl, K. A Liquid-Helium Cryostat for Collection of Three-

Dimensional X-Ray Intensity Data down to 20 K. The Crystal Structure of D (+)-Tartaric Acid at 35, 105, 160 and 295 K. *J. Appl. Crystallogr.* **1979**, *12* (6), 537–544. https://doi.org/10.1107/S0021889879013224.

(59) Roca-Paixão, L. Investigation of Pharmaceutical Multicomponent Systems: An Insight from Computational and Experimental Results, University of Lille, 2020.

(60) Lerbret, A.; Bordat, P.; Affouard, F.; Descamps, M.; Migliardo, F. How Homogeneous Are the Trehalose, Maltose, and Sucrose Water Solutions? An Insight from Molecular Dynamics Simulations. *J. Phys. Chem. B* **2005**, *109* (21), 11046–11057. https://doi.org/10.1021/jp0468657.

(61) Ottou Abe, M. T.; Viciosa, M. T.; Correia, N. T.; Affouard, F. Impact of Chirality on Peculiar Ibuprofen Molecular Dynamics: Hydrogen Bonding Organization and: Syn vs. Anti Carboxylic Group Conformations. *Phys. Chem. Chem. Phys.* **2018**, *20* (46), 29528–29538. https://doi.org/10.1039/C8CP04837A.

(62) Guerain, M.; Derollez, P.; Roca-Paixão, L.; Dejoie, C.; Correia, N. T.; Affouard, F. Structure Determination of a New Cocrystal of Carbamazepine and DL-Tartaric Acid by Synchrotron Powder X-Ray Diffraction. *Acta Crystallogr. Sect. C Struct. Chem.* **2020**, *76* (3), 225–230. https://doi.org/10.1107/S2053229620000868.

(63) M. J. Frisch, G. W. Trucks, H. B. Schlegel, G. E. Scuseria, M. A. Robb, J. R. Cheeseman, G. Scalmani, V. Barone, G. A. Petersson, H. Nakatsuji, X. Li, M. Caricato, A. Marenich, J. Bloino, B. G. Janesko, R. Gomperts, B. Mennucci, H. P. Hratchian, J. V. Ortiz, A. F. Izmaylov, J. L. Sonnenberg, D. Williams-Young, F. Ding, F. Lipparini, F. Egidi, J. Goings, B. Peng, A. Petrone, T. Henderson, D. Ranasinghe, V. G. Zakrzewski, J. Gao, N. Rega, G. Zheng, W. Liang, M. Hada, M. Ehara, K. Toyota, R. Fukuda, J. Hasegawa, M. Ishida, T. Nakajima, Y. Honda, O. Kitao, H. Nakai, T. Vreven, K. Throssell, J. A. Montgomery, Jr., J. E. Peralta, F. Ogliaro, M. Bearpark, J. J. Heyd, E. Brothers, K. N. Kudin, V. N. Staroverov, T. Keith, R. Kobayashi, J. Normand, K. Raghavachari, A. Rendell, J. C. Burant, S. S. Iyengar, J. Tomasi, M. Cossi, J. M. Millam, M. Klene, C. Adamo, R. Cammi, J. W. Ochterski, R. L. Martin, K. Morokuma, O. Farkas, J. B. Foresman, and D. J. Fox, Gaussian 09, Revision D.01, Gaussian, Inc.,Wallingford CT, 2016.

(64) Kremer, F.; Schönhals, A. *Broadband Dielectric Spectroscopy*; Kremer, F., Schönhals, A., Eds.; Springer Berlin Heidelberg: Berlin, Heidelberg, 2003. https://doi.org/10.1007/978-3-642-56120-7.

(65) Kremer, F.; Loidl, A. *The Scaling of Relaxation Processes*; Kremer, F., Loidl, A., Eds.; Advances in Dielectrics; Springer International Publishing: Cham, 2018. https://doi.org/10.1007/978-3-319-72706-6.

(66) Brand, R.; Lunkenheimer, P.; Loidl, A. Relaxation Dynamics in Plastic Crystals. *J. Chem. Phys.* **2002**, *116* (23), 10386–10401. https://doi.org/10.1063/1.1477186.

(67) Descamps, M.; Correia, N. T.; Derollez, P.; Danede, F.; Capet, F. Plastic and Glassy Crystal States of Caffeine. *J. Phys. Chem. B* **2005**, *109* (33), 16092–16098. https://doi.org/10.1021/jp040494c.

(68) Plaga, L. J.; Raidt, A.; Fuentes Landete, V.; Amann-Winkel, K.; Massani, B.; Gasser, T. M.; Gainaru, C.; Loerting, T.; Böhmer, R. Amorphous and Crystalline Ices Studied by Dielectric Spectroscopy. *J. Chem. Phys.* **2019**, *150* (24), 244501. https://doi.org/10.1063/1.5100785.

(69) Timmermans, J. Plastic Crystals: A Historical Review. *Journal of Physics and Chemistry of Solids*. 1961, pp 1–8. https://doi.org/10.1016/0022-3697(61)90076-2.

(70) Sherwood, J. N. *The Plastically Crystalline State:Orientationally Disordered Crystals*; Wiley: New York, 1979.

(71) Cole, K. S.; Cole, R. H. Dispersion and Absorption in Dielectrics I. Alternating Current Characteristics. *J. Chem. Phys.* **1941**, *9* (4), 341–351. https://doi.org/10.1063/1.1750906.

(72) Correia, N. T.; Moura Ramos, J. J. On the Cooperativity of the β-Relaxation: A Discussion Based on Dielectric Relaxation and Thermally Stimulated Depolarisation Currents Data. *Phys. Chem. Chem. Phys.* **2000**, *2* (24), 5712–5715. https://doi.org/10.1039/b005867j.

(73) Ngai, K. L. An Extended Coupling Model Description of the Evolution of Dynamics with Time in Supercooled Liquids and Ionic Conductors. *J. Phys. Condens. Matter* **2003**, *15* (11), S1107–S1125. https://doi.org/10.1088/0953-8984/15/11/332.

(74) Ngai, K. L. *Relaxation and Diffusion in Complex Systems*; Partially Ordered Systems; Springer New York: New York, NY, 2011. https://doi.org/10.1007/978-1-4419-7649-9.

(75) Kohlrausch, R. Nachtrag Uber Die Elastiche Nachwirkung Beim Cocon Und Glasladen. *Ann. Phys.* **1847**, *72* (393), 7.

(76) Kohlrausch, R. Theorie Des Elektrischen Rückstandes in Der Leidener Flasche. *Ann. der Phys. und Chemie* **1854**, *167* (1), 56–82. https://doi.org/10.1002/andp.18541670103.

(77) Williams, G.; Watts, D. C. Non-Symmetrical Dielectric Relaxation Behaviour Arising from a Simple Empirical Decay Function. *Trans. Faraday Soc.* **1970**, *66* (1), 80–85. https://doi.org/10.1039/TF9706600080.

(78) Alvarez, F.; Alegra, A.; Colmenero, J. Relationship between the Time-Domain Kohlrausch-Williams-Watts and Frequency-Domain Havriliak-Negami Relaxation Functions. *Phys. Rev. B* **1991**, *44* (14), 7306–7312. https://doi.org/10.1103/PhysRevB.44.7306.

(79) Kauzmann, W. The Nature of the Glassy State and the Behavior of Liquids at Low Temperatures. *Chem. Rev.* **1948**, *43* (2), 219–256. https://doi.org/10.1021/cr60135a002.

(80) Hodge, I. M. Strong and Fragile Liquids — a Brief Critique. *J. Non. Cryst. Solids* **1996**, *202* (1–2), 164–172. https://doi.org/10.1016/0022-3093(96)00151-2.

(81) Angell, C. A. Relaxation in Liquids, Polymers and Plastic Crystals - Strong/Fragile Patterns and Problems. *J. Non. Cryst. Solids* **1991**, *131–133* (PART 1), 13–31. https://doi.org/10.1016/0022-3093(91)90266-9.

(82) Affouard, F.; Correia, N. T. Debye Process in Ibuprofen Glass-Forming Liquid: Insights from Molecular Dynamics Simulation. *J. Phys. Chem. B* **2010**, *114* (35), 11397–11402. https://doi.org/10.1021/jp1046358.

(83) Böttcher, C. J. F. *Theory of Electric Polarization*; Elsevier, 1973; Vol. I. https://doi.org/10.1016/C2009-0-15579-4.

(84) Roca-Paixão, L.; Correia, N. T.; Affouard, F. Affinity Prediction Computations and Mechanosynthesis of Carbamazepine Based Cocrystals. *CrystEngComm* **2019**, *21* (45), 6991–7001. https://doi.org/10.1039/C9CE01160A.

(85) Smith, W. , Forester, T. R.; Todorov, I. T. *The DL POLY Classic User Manual*, 1.9.; http://docplayer.net/14320255-The-dl-poly-2-user-manual.html, 2012.

(86) Wang, J.; Wolf, R. M.; Caldwell, J. W.; Kollman, P. A.; Case, D. A. Development and Testing of a General Amber Force Field. *J. Comput. Chem.* **2004**, *25* (9), 1157–1174.

(87) Caleman, C.; Van Maaren, P. J.; Hong, M.; Hub, J. S.; Costa, L. T.; Van Der Spoel, D. Force Field Benchmark of Organic Liquids: Density, Enthalpy of Vaporization, Heat Capacities, Surface Tension, Isothermal Compressibility, Volumetric Expansion Coefficient, and Dielectric Constant. *J. Chem. Theory Comput.* **2012**, *8* (1), 61–74. https://doi.org/10.1021/ct200731v.

(88) Momma, K.; Izumi, F. VESTA 3 for Three-Dimensional Visualization of Crystal, Volumetric and Morphology Data. *J. Appl. Crystallogr.* **2011**, *44* (6), 1272–1276. https://doi.org/10.1107/S0021889811038970.

For Table of Contents Use Only

Title: Nature of the structural and dynamical disorder in organic cocrystals with a true nanometric size channel-like architecture

Authors: Luisa Roca-Paixão, Natália T. Correia, Florence Danède, Maria T. Viciosa, Alexander Lee Morritt, Yaroslav Z. Khimyak, Frédéric Affouard

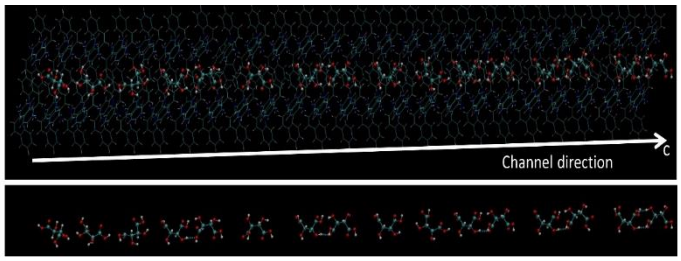

3.5 cm high x 9 cm wide

Synopsis consisting of 60 words or less

Molecular Dynamics simulations combined with experimental techniques highlight the nature of structural and dynamical disorder of tartaric acid (guest) molecules present in channels formed by carbamazepine (host matrix) in the carbamazepine-tartaric acid (3:1) cocrystal. Tartaric acid species that organized as one-dimension interrupted single files of molecules weakly hydrogen bonded to each other show rotational and translational dynamical disorder.